Studies on X-ray Interactions near K-edge using ^{241}Am source and Proton Induced X-ray Emission(PIXE)

Thesis submitted to the University of Calicut
in partial fulfillment of the requirements
for the the degree of

Doctor of Philosophy
in
Physics

K. K. Abdullah

Department of Physics
University of Calicut
P. O. Calicut University, PIN-673 635
Malappuram Dt., Kerala.

December 2007

CERTIFICATE

Certified that the work presented in this thesis entitled 'Studies on X-ray Interactions near K-edge using ^{241}Am source and Proton Induced X-ray Emission(PIXE)' is a bonafide work done by Mr. K. K. Abdullah, under my guidance in the Department of Physics, University of Calicut and that this work has not been included in any other thesis submitted previously for the award of any degree.

University of Calicut
December 2007

Prof. K. Muraleedhara Varier
(Supervising Guide)

DECLARATION

I hereby declare that the work presented in this thesis entitled 'Studies on X-ray Interactions near K-edge using ^{241}Am source and Proton Induced X-ray Emission(PIXE)' is based on the original work done by me under the guidance of Prof. K. Muraleedhara Varier, Department of Physics, University of Calicut, and has not been included in any other thesis submitted previously for the award of any degree.

University of Calicut
December 2007 K. K. Abdullah

Acknowledgements

Fling a pebble into a pond, and it makes ripples on the surface that move out from the point where the pebble entered the water. The waves grow larger in radius but gradually get attenuated as they move away. Electromagnetic radiations also do attenuate while passing through matter, but marked by abrupt variations of intensity around the absorption edges.

I was introduced to the exciting world of interaction of photons with matter by none other than Prof. K. Muraleedhara Varier, Head of the Department of Physics, University of Calicut, whose extensive knowledge and expertise in the subject guided me through this research work. His deep concern and involvement helped even to locate any missing spectrum from among the many recorded in the computer. I feel honoured to have worked under him, who cares to keep human values so close to his heart.

Prof. K. Neelakandan, retired head of the Department of Physics actually gave me an initial thrust to the field of research. I remain grateful to him for his kind words. Prof. B. R. S. Babu was genuinely interested to know the progress of the work and it is my pleasure to thank him for his valuable suggestions. I also thank all the faculty members, library and office staff of the Department for the help they rendered during the entire course of my research study.

Part of the research work was carried out at the Particle Irradiation Facility Section, Indira Gandhi Centre for Atomic Research, Kalpakkam, Tamil Nadu. I am deeply indebted to Dr. K. G. M. Nair, the head of the Section, for sanctioning beam time of 1.7 MV Tandetron Accelerator. I owe greatly to Mr. P. Magudapathy for rendering all the help in the PIXE measurements, providing necessary reference articles and arranging my stay at IGCAR.

I am deeply indebted to Prof. Govinda Nayak and Prof. Balakrishna, Dept. of Physics, Mangalore University for allowing the use of amerecium source. Let me also express my sincere thanks to Mr. B. P. Ajithkumar and Mr. E. T. Subramaniam of the Inter University Accelerator Centre, New Delhi for

providing the FREEDOM software for the analysis of data.

Farook College, Kozhikode ever remains in the forefront of academic enrichment of its faculty. The Management of the College, Prof. A. Kuttialikutty, Principal and Dr. P. M. Mubarak Pasha, former Principal deserve special mention for granting permission to undergo the course under the Faculty Improvement Programme. I would also like to thank my colleagues in the Department of Physics, Farook College for their keen interest and encouragement in my research work. Mr. K. A. Mathew, even accompanied me and helped a lot to take back the repaired HPGe detector from Bangalore.

I wish also to place on record my special thanks to the University Grants Commission, New Delhi, and also to the Government of Kerala for granting teacher fellowship and sanctioning deputation without which this work would have been impossible.

Research life in the University campus would have been miserable without the company of my co-researchers Udayanandan, Jeena, Sethumadhavan, Rajeevan, Rajeev Thomas and Bipin. We talked and argued over many topics at lunch and tea breaks speeding through the rocky, cashew-nut tree ridden southern part of the campus. I am really grateful to them for the delightful moments.

K.K.Abdullah

Contents

List of Figures

List of Tables

List of Photographs

Preface

X-ray attenuation coefficients and cross-sections are of great significance in both applied and fundamental science. They are invaluable in many applied fields, such as nuclear diagnostics, radiation protection, nuclear medicine, radiation dosimetry, etc. In recent years, there has been renewed interest in the measurement of photon interaction cross-sections at low energies, especially energies close to absorption edges of elements.

In the present work, X-ray attenuation coefficients are determined at different energies around K-edge of few elements using ^{241}Am source. Attenuation measurements were also done for some simple thin foil samples using radioactive source and Proton Induced X-ray Emission. Since anomalous scattering factor or of X-ray resonant scattering changes remarkably near an absorption edge of an atom in the energy region of present interest, the anomalous scattering factors $f'+\mathrm{i}f''$ were derived for few elements from the attenuation measurements.

The thesis is organized as follows: **Chapter 1** gives an introduction to the basic interactions of electromagnetic radiation with matter. The elastic and inelastic scattering, photoelectric absorption, absorption edges, dispersion correction, sources for radiation interaction studies including Proton Induced X-ray Emission(PIXE) are also briefly described. **Chapter 2** reviews the work already taken place in the field of X-ray attenuation measurements using radioactive sources as well as with PIXE. The related works on Dispersion correction is also reviewed in this chapter.

Chapter 3 describes the attenuation measurements carried out around K-edge of rare earth elements Sm, Eu, Gd, Tb, Dy and Er using 59.54 keV gamma

rays. The method of Compton scattering of the primary photons by an aluminum target is adopted to get continuously variable energy in the range from 49.38 keV to 57.96 keV. **Chapter 4** describes Proton Induced X-ray Emission(PIXE) and experimental determination of mass attenuation coefficients (μ/ρ) for elements Zr, Nb, Mo and Pd around their K-edges using the technique. The measurements were done at 14 energies in the range $15.744 - 28.564$ keV using secondary excitation from thin Zr, Nb, Mo, Rh, Pd, Cd and Sn foils at their K_α and K_β energy values.

Chapter 5 deals with the experimental determination of mass attenuation coefficients (μ/ρ) for elements Zr, Nb, Mo and Pd around their K-edges for the energy range $15.744 - 28.564$ keV, using ^{241}Am source. **Chapter 6** gives a brief theoretical background of the theory of anomalous scattering. The real and imaginary parts, f' and f'' of the dispersion corrections for the elements Zr, Nb, Mo and Pd have been determined by a numerical evaluation of the dispersion integral.

A summary of the results obtained and the future prospectives of the work are included at the end of the thesis.

List of papers published/presented/communicated:

1. Photon Interaction studies using ^{241}Am gamma rays - *Pramana Journal of Physics Vol. 67, No. 3 , September 2006.*

2. Simulated mixed absorbers and effective atomic numbers for gamma attenuation *Pramana Journal of Physics Vol. 67, No. 3 , September 2006.*

3. Attenuation studies near K-absorption edges using Compton scattered ^{241}Am gamma rays (*Accepted in Pramana Journal of Physics*)

4. X-ray attenuation around K-edge by Zr, Nb, Mo and Pd : A comparative study using PIXE and ^{241}Am gamma rays (*Communicated*)

5. Compton scattering : A versatile technique for attenuation studies around K-absorption edge - *National Symposium on Radiation Physics (NSRP-17), November 14-16, 2007 Saha Institute of Nuclear Physics, Kolkata.*

6. X-ray attenuation around K-edge by Zr, Nb, Mo and Pd: A comparative study using PIXE and ^{241}Am gamma rays - *National Symposium on Radiation Physics (NSRP-17), November 14-16, 2007 Saha Institute of Nuclear Physics, Kolkata.*

7. PIXE analysis of ground water in Eloor industrial belt in Kerala. - *Indian Particle Accelerator Conference, InPAC-2006, Nov 1- 4, 2006 BARC-TIFR, Mumbai.*

8. PIXE analysis of trace elements of blood samples from children with bronchial asthma - *Annual Conference on Medical Physics and Radiation Safety, 23-24 Sept 2006, VIT, Vellore, Tamil Nadu.*

9. PIXE analysis of trace elements of blood samples from chronic pancreatitis group - *Annual Conference on Medical Physics and Radiation Safety, 23-24 Sept 2006, VIT, Vellore, Tamil Nadu.*

Chapter 1

Interaction of Photons with matter

Electromagnetic radiation can be described in terms of a stream of photons, which are massless particles each traveling in a wave-like pattern and moving at the speed of light. Each photon contains a certain amount (or bundle) of energy, and all electromagnetic radiation consists of these photons. The only difference between the various types of electromagnetic radiation is the amount of energy found in the photons. Radio waves have photons with low energies, microwaves have a little more energy than radio waves, infrared has still more, then visible, ultraviolet, X-rays, and the most energetic of all, γ-rays.

The study of interaction of X-rays and γ-rays has drawn wide attention by virtue of its diverse applications in various fields of science and technology. X and γ interaction cross sections are essential in a variety of applications in medicine, biology, agriculture, industry, X-ray surveillance as well as in radiation calculations, industrial radiography, radiometric gauging etc. These high frequency radiations are classified according to their mode of origin, not by their energy. Thus γ-rays are the electromagnetic radiations accompanying nuclear transitions. Characteristics X-rays are emitted in atomic transitions of bound electrons between the K, L, M... shells in atoms. Interactions of these photons with matter are thought to be independent of the mode of origin of the photon and dependent only up on their quantum energy, $h\nu$. A number of possible

interaction mechanisms are known for interaction of radiation with matter. A catalogue of the possible processes by which the electromagnetic field of the γ and X-radiations may interact with matter has been put in the following form by Fano [1]

Kinds of interaction	*Effects of Interaction*
1. Interaction with atomic electrons	(a) Complete absorption
2. Interaction with nucleons	(b) Elastic scattering(coherent)
3. Interaction with the electric field surrounding nuclei or electrons	(c) Inelastic scattering(incoherent)
4. Interaction with the meson field surrounding nucleons	

There are 12 ways of combining columns 1 and 2; thus in theory there are 12 different processes of interaction which are generally classified into *Scattering* and *Absorption*. These processes lead to the partial or complete transfer of the photon energy. They result in sudden and abrupt changes in the photon history, in that the photon either disappears entirely or is scattered through a large average angle.

1.1 Scattering

Generally, *scattering* is a physical process whereby a beam of radiation is forced to deviate from a straight trajectory by one or more localized non-uniformities in the medium through which it passes. In physical descriptions of scattering, physicists commonly distinguish between two broad types, *elastic* and *inelastic.*

1.1.1 Elastic scattering

In *elastic scattering*, the gamma ray energy is unchanged, except for a negligible amount which is lost due to the recoil of the scattering nucleus, acquired by it for momentum conservation. The direction of propagation of the photon is changed by the potential of the target. In *Inelastic scattering*, there is a loss of

energy of the gamma ray; the scattering atom being excited by an amount equal to the energy lost by the gamma ray. *Thomson scattering* refers to the elastic scattering from the free electron or nucleus. If the scattering takes place from bound electron, then it is called the *Rayleigh scattering*. The contribution of nuclear scattering consists also of *Nuclear resonance scattering*. The interaction between the incident photons and the strong Coulomb field of the nucleus results in what is known as *Delbruck scattering*.

Thomson scattering

In *Thomson scattering* from a free electron, the oscillating electromagnetic field of the incident photon sets the electron into oscillations in the direction of its electric vector. The frequency of these oscillations is the same as those of the incident wave. The interaction results in the emission of electromagnetic waves of the same frequency (energy) as the incident photon. More exactly, energy is absorbed from the incident wave by the electron and re-emitted as electromagnetic radiation as shown in Figure 1.1. The electric fields of the incoming and

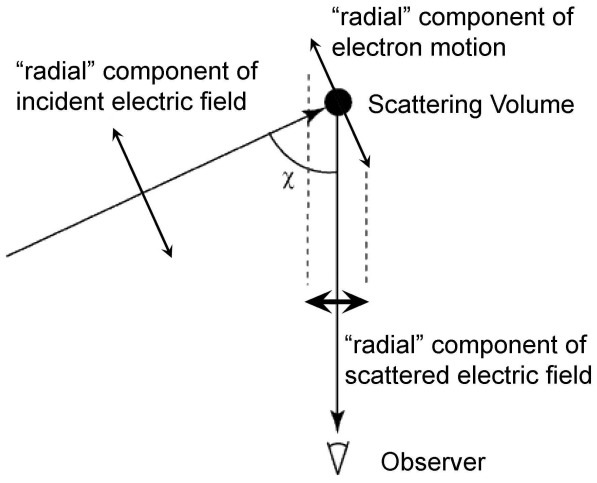

Figure 1.1: Thomson scattering of electromagnetic radiation by an electron.

observed beam can be divided up into those components lying in the plane of observation (formed by the incoming and observed beams) and those components

perpendicular to that plane. Those components lying in the plane are referred to as "radial" and those perpendicular to the plane are "tangential", since this is how they appear to the observer. The diagram shows the radial component of the incident electric field causing a component of motion of the charged particles at the scattering point which also lies in the plane of observation. The amplitude of the wave observed will be proportional to the cosine of χ, the angle between the incident and observed beams. The intensity, which is the square of the amplitude, will then be diminished by a factor of $cos^2\chi$. It can be seen that the tangential components (perpendicular to the plane of the diagram) will not be affected in this way. If the charged particle in question is an electron, the well known Thomson scattering cross section is given by

$$\sigma_{Thomson} = \frac{8\pi}{3}(e^2/4\pi\epsilon_0 m_e c^2) = 6.65 \times 10^{-29} m^2. \tag{1.1}$$

The quantity $(e^2/4\pi\epsilon_0 m_e c^2) = 2.8 \times 10^{-15}$m is called the classical electron radius (it is the radius of spherical shell of total charge whose electrostatic energy equals the rest mass energy of the electron). Electron, thus acts as a scatterer, rather like a solid sphere whose radius is of order the classical electron radius. Since this radius is extremely small, it is clear that scattering of radiation by a single electron (or any other charged particle) is a very weak process.

Rayleigh Scattering

Rayleigh scattering is essentially Thomson scattering on electrons bound in an atomic potential, including the effects of resonances and phase coherence between multiple electrons [2]. Here, the photons are scattered by the bound electrons in a process where the atom is eventually neither excited nor ionized. The atom is therefore left in its ground state itself after the scattering process. The scattering from different parts of the atomic cloud of electrons combine in phase to give coherent scattering. This process mainly occurs at low energies and for large Z values where the electron binding energies influence the Compton effect. In this scattering process, the energy (and therefore the wavelength) of the incident

photon is conserved and only its direction is changed and the scattering intensity is proportional to the fourth power of the reciprocal wavelength of the incident photon. Since the scattering is taking place with particles whose size is much smaller than the wavelength (λ) of the incident photon, the size of a scattering particle is defined by the ratio x of its characteristic dimension r to wavelength, as

$$x = \frac{2\pi}{r}\lambda. \tag{1.2}$$

The intensity I of light scattered by a single small particle from a beam of unpolarized light of wavelength λ and intensity I_0 is given by

$$I = I_0 \frac{1 + cos^2\theta}{2R^2}[(n^2 - 1)/(n^2 + 2)]^2(2\pi/\lambda)^4(d/2)^6, \tag{1.3}$$

where R is the distance to the particle, θ is the scattering angle, n is the refractive index of the particle, and d is the diameter of the particle. The angular distribution of Rayleigh scattering, governed by the $(1 + cos^2\theta)$ term, is symmetric in the plane normal to the incident direction of the light, and so the forward scatter equals the backwards scatter. Integrating over the sphere surrounding the particle, gives the Rayleigh scattering cross section

$$\sigma_s = \frac{2\pi^5}{3}(d^6/\lambda)^4[(n^2 - 1)/(n^2 + 2)]^2. \tag{1.4}$$

Rayleigh scattering can occur when light travels in transparent solids and liquids, but is most prominently seen in gases. The familiar blue colour of sky is also due to Rayleigh scattering of sunlight.

Nuclear resonance scattering

In the case of *nuclear resonance scattering*, the incident photon excites the nucleus to one of its excited levels. It is subsequently de-excited by re-emission of the excitation energy in the form of a gamma quantum. Thus, the emitted gamma energy will be nearly equal to that of the incident photon except for a negligible loss due to the recoil of the nucleus. The cross section is very small

unless the gamma energy happens to be close to one of the energy levels of the nucleus. It has a clear resonance behaviour with full width at half maximum (FWHM) characterized by the energy width of the nuclear level with energy E_0 involved in the process. The cross section in this case has an energy dependence as follows:

$$\sigma_{NR} = \lambda^2 \Gamma \Gamma_\gamma / 4\pi [(E_0 - E_\gamma)^2 + (\Gamma/2)^2]. \tag{1.5}$$

Here, λ is the incident photon wavelength, Γ is the total width of the nuclear level, Γ_γ is the partial width for gamma decay of the excited state of energy and E_γ is the photon energy. Due to the comparatively narrow widths of nuclear levels at low excitations, the chance of overlap of the incident gamma energy with the excitation energy of the target nucleus is very rare indeed. Therefore, unless there is an accidental overlap of E_γ with E_0, the contribution from nuclear resonance scattering process to the observed elastic scattering of the incident photons is negligible. Apart from the above mentioned nuclear resonance scattering process, there is yet another resonance process of nuclear scattering which the incident photon can undergo. A strong photon absorption is observed for many nuclei near gamma energies given by

$$E_0 = \epsilon A^{-1/3} \tag{1.6}$$

where ϵ varies between 70 to 80 MeV and A is the atomic number of the element. The scattering then corresponds to the *Giant Dipole Resonance scattering* (GDR). The process is appreciable only at energies above 10 MeV or so. However, the resonance being very broad, the low energy tail of the resonance peak can contribute to the elastic scattering at lower energies also.

Delbruck scattering

Delbruck scattering, also known as the *elastic nuclear potential scattering* is due to virtual electron pair formation in the nuclear Coulomb field. The actual mechanism of the process involves the absorption of the incident photon by an

electron in the negative energy state, followed by the creation of a electron-positron pair and subsequent annihilation of the pair to give a scattered photon of exactly the same energy as the incident photon. The cross section is very small at low gamma energies below 1 MeV, but increases at higher energies. It has a dependence on the atomic number of the scatterer. The real part of the scattering amplitude is related to virtual pair production in the intermediate state. The imaginary part of the scattering amplitude corresponds to real pair production in the intermediate state. Of course, real pair production is possible only if the incident photon energy is above the pair production threshold of 1.022 MeV.

1.1.2 Inelastic scattering

In particle physics and chemistry, *inelastic scattering* is a fundamental scattering process in which the kinetic energy of an incident particle is not conserved. In this scattering process, the energy of the incident particle is lost or gained. When a photon is the incident particle, the inelastic scattering process is called *Raman scattering* wherein the incident photon interacts with matter (gas, liquid, and solid) and the frequency of the photon is shifted to blue or red. The blue shift can be observed when the internal energy of matter is transferred to the photon; this process is called *anti-Stokes Raman scattering*. The red shift can be observed when a part of the energy of the photon is changed to the internal energy of the interacting matter; this process is called *Stokes Raman scattering*.

Inelastic scattering also occurs in the interaction between an electron and a photon. When a high energy photon collides with a free electron and transfers energy, the process is called *Compton scattering*. Furthermore, when an electron with relativistic energy collides with an infrared or visible photon, the electron gives energy to the photon; this process is called *inverse-Compton scattering*.

Compton scattering

In *Compton scattering*, which is the most common type of inelestic scattering, the incoming γ-ray photon is deflected through an angle θ with respect to its original direction as shown in Figure 1.2. The photon transfers a portion of its

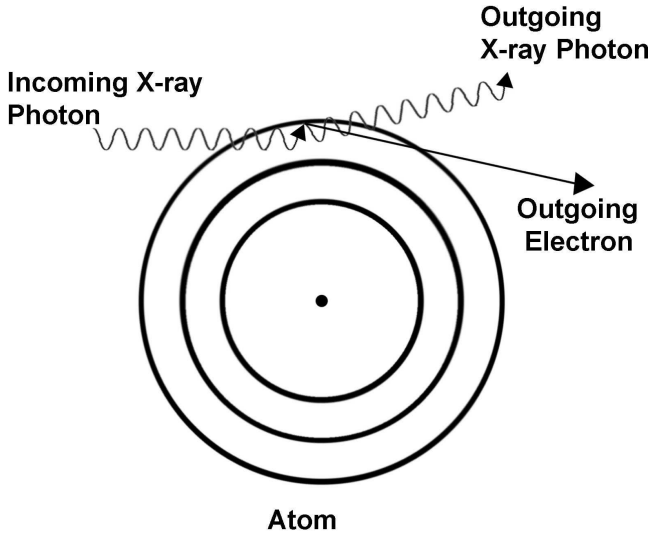

Figure 1.2: Compton scattering of X-rays from atomic electrons in a target.

energy to the electron (assumed to be initially at rest), which is then known as a recoil electron. Since all angles of scattering are possible, the energy transferred to the electron can vary from zero to a large fraction of the γ-ray energy. The equation which relates the energy transfer and the scattering angle for any given interaction can be written as

$$h\nu' = \frac{h\nu}{1 + (h\nu/m_0c^2)(1 - cos\theta)}, \tag{1.7}$$

where $h\nu$ and $h\nu'$ are the energies of the incident and deflected photons, h is the Plank's constant, m_o is the rest mass energy of the electron, c is the velocity of light and θ is the angle of scatter of photon relative to its original direction of travel. The above equation can be re-written in terms of the wavelengths of the incident and scattered photons as

$$\lambda_f - \lambda_i = \Delta\lambda = \frac{h}{m_0c}(1 - cos\theta), \tag{1.8}$$

where h is the Planck's constant. This shift in wavelength is called the *Compton shift* and is seen to be independent of the wavelength of the incident radiation. The cross section for the Compton scattering from a free electron has been derived by Klein and Nishina [3] based on Dirac's relativistic theory of the electron. Their result is embodied in the famous Klein-Nishina formula,

$$\frac{d\sigma}{d\Omega} = r_0^2[\frac{1}{1+\alpha(1-cos\theta)}]^3[\frac{1+cos^2\theta}{2}][1+\frac{\alpha^2(1-cos\theta)^2}{(1+cos^2\theta)[1+\alpha(1-cos\theta)]}], \quad (1.9)$$

where $\alpha \equiv h\nu/m_0c^2$ and r_0 is the classical electron radius.

1.2 Absorption

If the radiation is substantially or completely extinguished by the interaction (losing a significant proportion of its energy), the process is known as *absorption*. In some contexts, absorption is considered to be merely an extreme form of inelastic scattering. Generally speaking, in classical physics, absorption and scattering tend to be treated as different phenomena, while in quantum physics absorption is treated as a form of scattering via the S-matrix. To be precise, absorption cannot occur without some degree of scattering, and scattering is rarely completely elastic in a microscopic scale.

1.2.1 Photoelectric effect

In the photoelectric absorption process, an incoming gamma photon interacts with and transfers its energy to an atomic electron, ejecting that electron from the atom as shown in Figure 1.3. The kinetic energy (E_e) of the resulting photoelectron is equal to the energy of the incident gamma photon minus the binding energy (E_e) of the electron and is given by

$$E_e = h\nu - E_b. \quad (1.10)$$

The photoelectric interaction is with the atom as a whole and cannot take place with free electrons. For γ-rays of sufficient energy, the most probable origin of

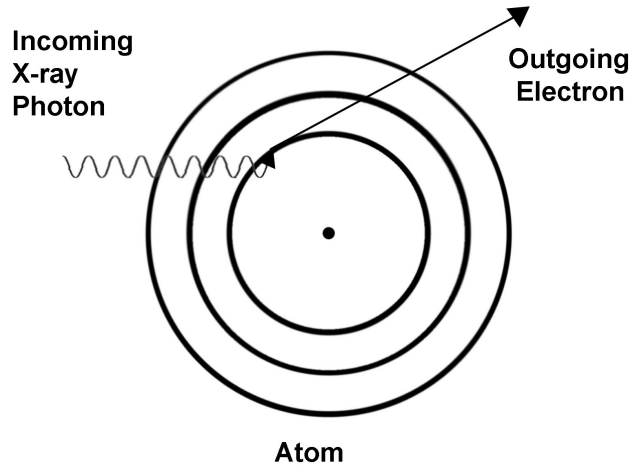

Figure 1.3: One of the atom's electrons absorbs the X-ray photon and is tossed completely out of the atom.

the photoelectron is the most tightly bound shell (K-shell) of the atom. The probability of photoelectric absorption per atom over all ranges of E_γ and Z s given by

$$\tau = Const. \times \frac{Z^n}{E_\gamma^3}, \tag{1.11}$$

where the exponent n varies between 4 and 5 over the γ-ray energy region of interest. Because of the strong dependence of photoelectric absorption probability on the atomic number Z, high Z materials are preferred for gamma ray detectors. The strong inverse dependence of τ on the γ-ray energy makes the photoelectric effect the predominant mode of interaction for the low energy γ-rays and X-rays.

Absorption edges

In the plot of mass attenuation coefficient, with incident γ-ray energy, discontinuities in the curve or "absorption edges" appear at energies which correspond to the binding energies of the electrons in the various shells of the absorber atom. The edge lying highest in energy therefore corresponds to the binding energy of K shell electron. For γ-ray energies slightly above the edge, the photon energy is just sufficient to undergo a photoelectric interaction in which K-electron is ejected from the atom. For gamma ray energies slightly below the edge, this process is

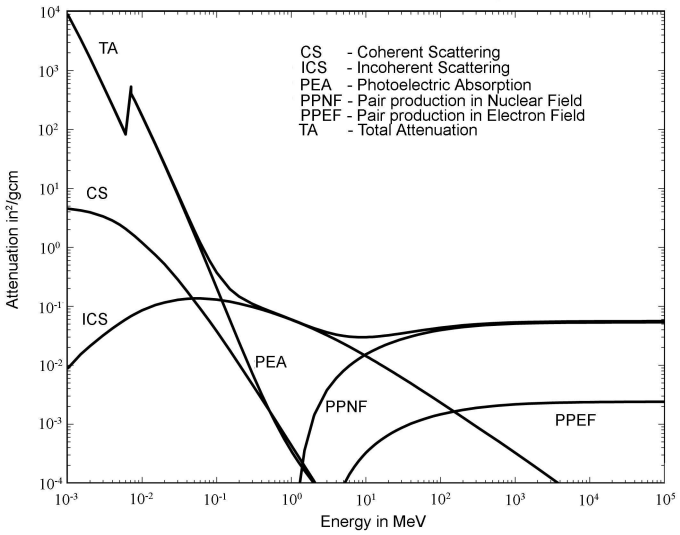

Figure 1.4: Energy dependence of the various gamma ray interaction processes in Fe.

no longer possible and therefore the interaction probability drops abruptly as illustrated in Figure 1.4. Similar absorption edges occur at lower energies for the L, M,..... electron shells of the atom also.

1.2.2 Pair production

In *pair production*, the entire gamma energy is completely absorbed in the material and used up in the creation of an electron-positron pair. The process can be represented as follows.

$$\gamma \longrightarrow e^- + e^+. \tag{1.12}$$

The energy balance equation can be written as

$$E\gamma = 2m_0c^2 + T_e^- + T_e^+, \tag{1.13}$$

where m_0 is the rest mass of the electron, T_e^- and T_e^+ are the kinetic energies of the electron and positron respectively. It is thus seen that pair production has a threshold energy given by $2m_0c^2 = 1.022$ MeV. Thus the process is possible only for gamma energies above 1.022 MeV. Above this threshold, the cross section for

the process increases and at higher energies, pair production is the predominant interaction.

The relative importance of the three processes namely photoelectric absorption, Compton scattering and pair production for different absorber materials and gamma ray energies is conveniently illustrated in Figure 1.5. The line at the left represents the energy at which photoelectric absorption and Compton scattering are equally probable as a function of the atomic number [4]. The line

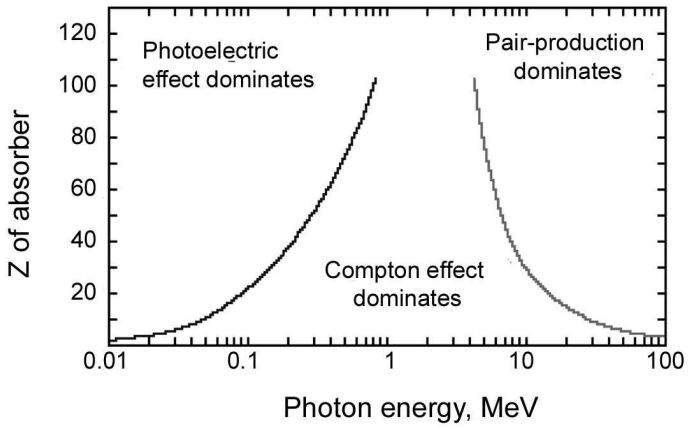

Figure 1.5: The energy dependence of the three major types of gamma ray interactions. The lines show the values of Z and $h\nu$ for which the two neighbouring effects are just equal.

at the right represents the energy at which Compton scattering and pair production are equally probable. Three areas are thus defined on the plot within which photoelectric absorption, Compton scattering and pair production dominate.

1.3 Attenuation

1.3.1 Beer-Lambert Formula

Attenuation is the reduction in intensity of the primary X-ray beam as it traverses matter by either absorption or scattering. When gamma rays pass through

matter, their intensity is attenuated according to the familiar exponential law. This means that a beam of radiation of a definite energy E_γ having intensity I_0, passing through an absorber of thickness x will have a transmitted intensity given by

$$I(x) = I_0 e^{-\mu x}, \tag{1.14}$$

where μ is a constant characterizing the medium for that gamma energy. It is called the *linear attenuation coefficient*. It represents sum of the probability per unit path length that the γ ray photon is removed from the beam due to photoelectric Compton scattering and pair production interactions. i.e.,

$$\mu = \tau(photoelectric) + \sigma(Compton) + \kappa(pair). \tag{1.15}$$

If x is in cm, μ will be expressed in units of cm^{-1}. The *mass attenuation coefficient* is expressed as (μ/ρ), where ρ is the density of the medium. It is more common to express the thickness of the absorber as $t = x\rho$, and the mass attenuation coefficient in units of cm^2/g. The absorption law can be rewritten as

$$I(t) = I_0 e^{(-\mu/\rho)t}, \tag{1.16}$$

which is known as *Beer-Lambert* formula. The exponential decrease of the gamma ray intensity arises from the fundamental nature of the interactions of the gamma rays with matter. When a gamma ray photon undergoes an interaction, it is either absorbed completely or scattered away from the incident direction. The probability for the interaction essentially depends on the number of interaction centers in the path of the gamma rays as well as on the probability for the interaction. If the incident gamma ray beam, having I photons traverses through a certain thickness x of the medium, let dI photons undergo interactions with the medium thereby getting removed from the direct beam. Then

$$\frac{dI}{I} = \frac{N_0 \rho \sigma dx}{A}, \tag{1.17}$$

where σ is the total cross section for all interactions and A is the mass number of the element of the medium (considering that the medium contains only one

element). N_0 is the Avogadro number. Letting $\mu = (N_0\rho\sigma)/A$ and integrating the above equation, we get back to eq.(1.16).

When a beam of gamma rays passes through an absorber, the gamma ray photons interact with the atoms individually and are either absorbed (via photoelectric effect and pair production) or scattered away from the beam. The intensity of the transmitted beam is consequently attenuated. The total cross section for attenuation of the incident beam of gamma rays is the sum of the cross sections per atom for all the three processes. Therefore, the total cross section is given by

$$\sigma = \sigma_\tau + \sigma_C + \sigma_{PP}. \tag{1.18}$$

If N is the number of atoms per unit volume of the absorber, the linear absorption coefficient can be written as

$$\mu = N\sigma. \tag{1.19}$$

1.3.2 Mixture rule

The linear absorption coefficient depends on the gamma ray energy E_γ, the atomic number Z and the density of the absorber medium. On the other hand, the mass attenuation co-efficient is independent of the absorber density. It depends only on the number of interacting centers in the path of the photon beam. Thus, for a mixture or a compound of different elements, the mixture rule [5] can be applied. The mass attenuation coefficient of a compound or mixture, according to the rule is

$$(\mu/\rho) = \sum_i w_i(\mu/\rho)_i, \tag{1.20}$$

where w_i is the proportion by weight of the element with mass absorption coefficient $(\mu/\rho)_i$.

1.3.3 Narrow beam and broad beam geometries

In order to find the value of μ, we have to know the initial intensity of the incident gamma ray photon, I_0. The absorption of gamma rays depends strongly upon its energy and the atomic number of the absorber. The exponential absorption law (eq.1.16) is difficult to observe experimentally, because of the detection of the gamma rays scattered from the absorber and other surrounding materials along with the transmitted beam. The X-rays emitted from the absorber also affect the measurements. In order to reduce the above mentioned problem we have to use a special geometry called *narrow beam geometry* set up. This arrangement reduces the solid angle subtended by the detector at the center of the target by use of suitable shielding and collimation. It prevents the coherently and incoherently scattered photons from reaching the detector. Hence only the radiation coming out from the target without any interaction will reach the detector. The Figure 1.6(a) below illustrates the narrow beam geometry compared to broad beam geometry.

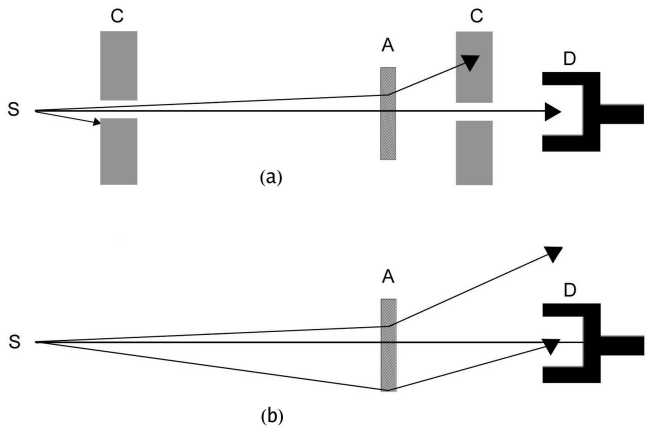

Figure 1.6: **(a)**-Narrow beam geometry **(b)**-Broad beam geometry; **S**-source, **C**-Collimator, **A**-Absorber, **D**-Detector.

Whenever a significant fraction of the scattered photons and the secondary photons can reach the detector, the arrangement is called *broad beam* or *poor geometry*, as shown in Figure 1.6(b). Here, there is no shielding for either

the source or the detector. The absorber to detector distance is comparatively smaller. Scattered radiation from the absorber can reach the detector within a reasonably large angle (the so called in-scattering angle). Thus, we will be detecting not only the purely transmitted photons but also those which have undergone scattering interactions. As a result the value of the measured attenuation coefficient will be smaller than the true value. Of course, one can still extract the true value of the attenuation coefficient provided a correction is applied for the in-scattering.

On the other hand, in the narrow beam geometry set up depicted in Figure 1.6(a), both the source and the detector are well shielded and the incident and transmitted beams are well collimated. The distances involved are also larger as compared to the broad beam geometry. The in-scattering angle is thereby minimized and the contribution of the scattered radiation will be negligible. Hence we get a value for the attenuation coefficient very near to the true value.

1.3.4 Buildup factor

In the broad beam geometry, the transmitted intensity of the gamma rays will not follow the normal exponential attenuation as given by eq.(1.16). Instead, we get the following equation

$$I(t) = B(t, E_\gamma) I_0 e^{(-\mu/\rho)t}. \tag{1.21}$$

Here, $B(t, E_\gamma)$ is a factor which accounts for the in-scattering. It depends on the in-scattering angle as well as on the absorber thickness and is called the buildup factor. The exponential term is retained to describe the major variation in the γ-ray counting rate with absorber thickness and the buildup factor is introduced as a multiplicative correction. The magnitude of the build up factor depends on the type of γ-ray detector used, because this will affect the relative weightage of the direct and scattered γ-rays. (With detector that responds only to the direct γ-rays, the build up factor is unity.) The build up also depends on the specific geometry of the experiment. As a rule of thumb, the build up factor of thick slab

absorbers tends to be about equal to the thickness of the absorber measured in units of mean free path of the incident γ-rays, provided the detector responds to broad range of γ-ray energies.

1.4 Proton Induced X-ray Emission(PIXE)

Proton induced X-ray emission (PIXE) technique [6, 7]relies on the analysis of the energy spectra of characteristic X-rays emitted from a sample bombarded with 1-3 MeV protons. The technique is widely used in different areas due to its possibilities in performing fast multi-elemental and nondestructive analysis of different kinds of samples. However, to convert the X-ray yields of different constituents of a thick sample to their concentrations, the X-ray mass attenuation coefficients are needed [8]. Knowledge of mass attenuation coefficients is also necessary in PIXE practice [9] to calculate the transmission of X-ray filters and also for an accurate Si(Li) detector efficiency determination [10], especially for low-energy X-rays (below 5 keV).

PIXE analysis consists of two parts. The first is to identify the atomic species in the target from the energies of the characteristic peaks in the X-ray emission spectrum and the second part is to determine the amount of a particular element present in the target from the intensity of its characteristic X-ray emission spectrum. This normally requires knowledge of the ionization cross-sections, fluorescence yields and absorption coefficients. In carrying out attenuation measurements in the X-ray region using PIXE facility, the samples are kept in a vacuum chamber are irradiated with $1-3$ MeV proton beam and the characteristic X-ray spectra are registered with a Si(Li) semiconductor detector coupled to standard electronics and a PC based multichannel analyzer. The spectra are analyzed by noting the component peaks of the X-ray spectrum for each absorber.

The major advantage of the PIXE technique is a low background yielding high sensitivity for trace element determination. The elements which are present

in the level of μg/g (ppm) or less generally considered as trace elements. Investigations for the determination of trace elements in biological specimen [11, 12] and also in environmental samples [13] using PIXE has been the subject of numerous research works for over 25 years.

1.5 Anomalous scattering factors

The effects of anomalous scattering which manifest themselves most when the incident X-ray energy approaches the absorption edge energies of an atom are described mathematically by two correction terms which are applied to the normal atomic form factor or Thompson scattering factor f_0. The modified scattering factor is given by

$$f = f_0 + f^{'} + if^{"} \tag{1.22}$$

where the first term f_0 is Thomson scattering factor, $f^{'}$ and $f^{"}$ are real and imaginary parts of anomalous scattering factors also known as the dispersion corrections to f_0. They give the deviation of the forward Raleigh scattering amplitude from the form factor. The optical theorem [14] demonstrates that the imaginary term $f^{"}$ is directly related to the atomic cross section as

$$f^{"} = \frac{E}{2hcr_0}\sigma_{tot}. \tag{1.23}$$

where $r_0 = \frac{e^2}{4\pi\epsilon_0 mc^2}$ is the classical electron radius, also known as the Compton radius or the Thomson scattering length which is based on a classical relativistic model of the electron. As in other resonance phenomena such as dielectric susceptibility, the real part of the dispersive term is related to the imaginary part by a Kramers-Kronig (K-K) transformation [15, 16]. In the case of X-ray scattering, the K-K transform takes the following form

$$f^{'}(Eo) = \frac{2}{\pi}\int_0^\infty \frac{Ef^{"}(E)}{E_0^2 - E^2}dE \tag{1.24}$$

In the energy region of current interest, if we neglect the spin flip processes, the $f^{'}$ and $f^{"}$ are connected by the modified Kramers-Kronig transform [17, 18, 19]

as given by

$$f^{'}(Eo) = f'(\infty) - \frac{2}{\pi} P \int_0^{\infty} \frac{E f^{"}(E)}{E_0^2 - E^2} dE \tag{1.25}$$

where $f'(\infty)$ is the high-energy limit and P is the Cauchy principal value of the dispersion integral, E_0 is the energy of interest. Thus, it is possible to determine the dispersion corrections $f^{'}$ and $f^{"}$ from a set of photoeffect cross sections using equations 1.24 and 1.25. The anomalous scattering factors are very much in need when performing Multiple wavelength Anomalous Diffraction (MAD) experiments.

1.6 XCOM

Berger and Hubbell [20, 21] developed a computer program, called XCOM, and a database which can be used to calculate cross sections and attenuation coefficients for any element, compound or mixture, at energies from 1 to 100 GeV. This, much used program has since undergone a number of updates, and is now also available in a Web version [22]. XCOM can generate cross sections and attenuation coefficients on a standard energy grid, spaced approximately logarithmically, or on a grid selected by the user, or for a mix of both grids. The program provides total cross sections and attenuation coefficients as well as partial cross sections for incoherent scattering, coherent scattering, photoelectric absorption, and pair production. For compounds, the quantities tabulated are partial and total mass interaction coefficients. Total attenuation coefficients without the contribution from coherent scattering are also given, because they are often used in gamma-ray transport calculations. Written in 1987, XCOM was intended to be compiled and linked on a main-frame computer, or run on a personal computer using the DOS operating system. The attenuation measurements in the present work on rare earth elements and thin foils obtained by using ^{241}Am source and Proton induced x-ray emission are compared with XCOM values and are plotted in the forthcoming chapters.

1.7 The present work

The broad aim of the present work is threefold :

I. Study X-ray attenuation of few rare earth elements with $62 \leq Z \leq 68$, by Compton scattering method.

We have carried out photon attenuation measurements at several energies in the range from 49.38 keV to 57.96 keV around the K-absorption edges of the rare earth elements Sm, Eu, Gd, Tb, Dy and Er using 59.54 keV γ-rays from ^{241}Am (300mCi) source after Compton scattering from an aluminium target. Pellets of oxides of the rare earth elements were chosen as mixture absorbers in these investigations. Under the narrow beam good geometry set up, the transmitted γ-rays were detected by an HPGe detector.

II. Study X-ray attenuation of few elements with $40 \leq Z \leq 46$ by using:

(a) Radioactive source and

(b) Proton Induced X-ray Emission.

Mass attenuation coefficients (μ/ρ) for elements Zr, Nb, Mo and Pd around their K-edges were measured at 14 energies in the range $15.744 - 28.564$ keV using secondary γ-ray excitation from thin Zr, Nb, Mo, Rh, Pd, Cd and Sn foils. These measurements were carried out at the K_α and K_β energy values of the target elements by two different techniques.

In the PIXE method, 2 MeV proton excited X-rays were used and detected by a Si(Li) detector of resolution 175 eV at 5.9 keV. In the second case, X-rays excited from the targets by 59.54 keV photons were detected by an HPGe detector.

III. Obtain anomalous scattering factors (dispersion corrections) to the forward Raleigh scattering amplitude for the elements with $40 \leq Z \leq 46$. Atomic photoeffect being an important process contributing to the total attenuation of the incident photon beam in the low energy region, our experimental data is used to find the anomalous scattering factors to the forward Raleigh scattering amplitude to the elements Zr, Nb, Mo and Pd.

References

[1] U. Fano, *Nucleonics*, **11**(8):8(1953); **11**(9):55(1953). [Chap.23, Introd.; Chap. 25, Secs. 1,3]

[2] L. Kissel, *Radiat. Phys. Chem.* **59**, 185 (2000).

[3] O. Klein and Y. Nishina, *Z. Physik*, **52**, 853 (1929).

[4] G. F. Knoll, *Radiation Detection and Measurement John Wiley and Sons, New York*, (1970).

[5] R. D. Evans, *The Atomic nucleus*, Mcgraw-Hill, New York, (1955).

[6] S. A. E. Johansson and J. L. Campbell, *PIXE, A Novel Technique for Elemental Analysis, Wiley, Chichester UK*, (1988).

[7] V. Havranek, V. Hnatowicz, J. Kvitek and I. Obrusnik, *Nucl. Instr. and Methods.* **B85**, 637 (1994).

[8] J. L. Campbell and J. A. Cookson, *Nucl. Instr. and Methods* **B3**, 185 (1984).

[9] K. M. Varier and M. P. Unnikrishinan, *Phys.Rev.A* **33**, 2382 (1986).

[10] M. Pajek, A. P. Kobzev, R. Sandrik, R. I. khamov and S. Khusumurodov, *Nucl. Instr. and Methods B* **42**, 346 (1989).

[11] K. K. Abdullah, K. M. Varier, R. E. Manikandan, Ananth N. Rao, P. Magudapathy and K. G. M. Nair, *Annual Conference on Medical Physics and Radiation Safety, 23-24 Sept 2006* VIT, Vellore, Tamil Nadu.

[12] K. K. Abdullah, K. M. Varier , R. E. Manikandan, Lulu Mathews, P. Magudapathy and K. G. M. Nair, *Annual Conference on Medical Physics and Radiation Safety, 23-24 Sept 2006* VIT, Vellore, Tamil Nadu.

[13] K. K. Abdullah, R. E. Manikandan, P. Magudapathy, K. G. M. Nair and K. M. Varier, *Indian Particle Accelerator Conference, InPAC-2006* Nov 1-4, 2006 BARC-TIFR, Mumbai.

[14] R. W. James, *The Optical Principles of the Diffraction of X-rays, G. Bell and sons Ltd, London*, (1969).

[15] H. A. Kramers, Cong. Intern. Fisica, (Transactions of Volta Centenary Congress) Como, **2**, 545 (1927).

[16] R. de L. Kronig, *J. Opt. Soc. Am.* **12**, 547(1926).

[17] B. Zhou, L. Kissel and R. H. Pratt, *Nucl. Instrum. Methods B* **66**, 307 (1992).

[18] B. L. Henke, P. Lee, T. J. Tanaka, R. L. Shimambukuro and B. K. Fujikawa, *At. Data Nucl. Data Tables* **27**, 1 (1982);

[19] B. L. Henke, E. M. Gullikson and J. C. Davis, *At. Data Nucl.Data Tables* **54**, 181(1993).

[20] J. H. Hubbell, *Natl. Stand. Ref. Data Ser.* **29** (1969).

[21] M. J. Berger and J. H. Hubbell, *National Bureau of Standards (former name of NIST), Gaithersburg, MD, "XCOM: Photon Cross Sections on a Personal Computer," NBSIR* 87-3597.

[22] M. J. Berger and J. H. Hubbell, *NIST Standard Reference Database 8, Version 1.1.2, National Institute of Standards and Technology, Gaithersburg, MD* (1999).

Chapter 2

Review of photon attenuation measurements

2.1 Introduction

Studies on photon attenuation measurements have so far been, primarily aimed to arrive at quite reasonable values of attenuation coefficients and cross sections that deviate a minimum from theory. The basic components of measurements on attenuation being source, detector and the absorbing medium, these studies involve number of variations on the nature and geometry of these components for making the results more refined. The present chapter reviews some of the attempts related to the photon attenuation measurements on elemental and compound substances using radioactive sources, secondary excited photons, parametric X-rays, discrete photons and proton induced X-ray emission (PIXE). Works already done around K-absorption edge, invoking mixture rule are also discussed. The photoeffect cross section σ being an important parameter in the low energy region, some of the related works on anomalous scattering factors are also reviewed.

2.2 Attenuation and Cross section measurements - Early days

Low-energy photons are used in basic as well as applied sciences. These applications span from computerized tomography to transmission/reflection experiments for studying composition of ancient coins in archaeometry. All these applications of X-rays require an accurate knowledge of the probabilities of various interactions of photons with matter. For this purpose, the available data of mass attenuation coefficients are normally used. Experimental measurements of the mass attenuation coefficients have been performed since the early days of X-ray studies and an almost complete collection, including also a comparison with theoretical predictions was reported by several authors, not least of which are the references; Storm and Israel [1], Hubbell [2], Henke *et al.* [3] and Saloman *et al.* [4].

Data on the scattering and absorption of photons (X-rays and gamma rays) are required for many scientific, engineering and medical applications. Available tables usually include cross sections for selected elements and possibly a limited number of compounds and mixtures. A convenient alternative to manual calculations, using tabulated data, is to generate cross sections and attenuation coefficients for elements, compounds and mixtures as needed, using a computer. For this purpose, Berger and Hubbell [5] developed a computer program, called XCOM, and a database which can be used to calculate cross sections and attenuation coefficients for any element, compound or mixture. It covers photon energies from 1 keV to 100 GeV, atomic numbers from 1 to 94 and edge positions, jumps and scattering coefficients, but no shell and subshell cross-sections. Gerward *et al.* [6] have developed a Windows version of XCOM called WinXCOM. Orlic *et al.* [7] have developed an interactive MS Windows based computer program for generating, printing and displaying mass attenuation coefficients.

The National Bureau of Standards (NBS) database provide experimental X-ray attenuation coefficients (total absorption cross sections) and cross sections,

calculated using a relativistic Hartree-Slater model for the photoelectric cross section for all elements of atomic number Z = 1-92 for the energy ranges 0.1-100 keV [8]. They have displayed the information in both tabular and graphical form. The X-ray mass attenuation coefficients of Veigele [9] have been parameterized by Braziewicz *et al.* [10] in the photon energy range of 1-150 keV for all elements from hydrogen to plutonium (Z = 1-94), taking into account the K-, M- and N-shell absorption edge structure existing in this energy interval. Hubbell has also compiled mass attenuation coefficients (μ/ρ) and mass energy-absorption coefficients (μ_n/ρ) and tabulated these quantities in units of m^2kg^{-1} for photon energies 1 keV to 20 MeV for 40 elements ranging from hydrogen (Z= 1) to uranium (Z= 92). In addition, these parameters are tabulated over this same energy range for 45 mixtures and compounds of dosimetric interest, computed from the above data using fractions-by-weight of the constituent elements. A bibliography of 290 references containing measured absolute-value photon total cross-section data above 10 eV is presented, by the same author. An index by element (Z = 1 to Z = 94) and energy range, characterizing experiments according to source, detector, and number of data points, is also included [11].

Gamma ray interaction studies at energies near the photo electric absorption edges have been of interest to investigators in the field for quite some time now [12, 13]. The energy region near the photo electric absorption edge in elements is interesting for many reasons. One reason is the validity of the mixture rule (referred to above) for the attenuation coefficients at energies close to the absorption edges [14]. This rule is valid when the effects on the atomic wave functions of the molecular bonding and chemical or crystalline environment are negligible. The attenuation coefficient values are believed to be affected by chemical, molecular and thermal environments. These phenomena lead to deviations of observed (μ/ρ) values from theoretical ones.

The measurements on attenuation of photons carried out in the present work are done around the K-edge of elements. In order to study the X-ray interaction processes near the absorption edges, one requires several radiation energies

around the edge energy.

There are five different techniques to obtain the required X-ray energies. They are :

I. Methods involving discrete energy radiations

a) Method using radioactive sources

b) Using secondary X-rays excited from elemental targets by photons from radioactive sources

c) Using secondary X-rays excited from elemental targets by the Proton Induced X-ray Emission (PIXE) Technique

II. Methods involving continuously variable energy radiations

d) By Compton scattering from a suitable target

e) Using Parametric X-ray Emission technique

The works already taken place with the techniques mentioned above are reviewed in the forthcoming section.

2.3 Methods involving discrete energy radiations

2.3.1 Methods using radioactive sources

The most straightforward method is to use different radioactive sources which provide discrete X-ray energies, namely the characteristic X-rays of the daughter isotopes. However, availability of such sources is limited. The intensities of X-rays available from such sources also are comparatively low for scattering studies and photo electric measurements, though they may be sufficient for attenuation measurements. Recently in our laboratory we had carried out investigations [15] on the attenuation coefficients and photoelectric effect on rare earth elements using ^{241}Am gamma rays. Appaji Gowda *et al.* [16, 17] have determined the attenuation coefficients for tantalum, mercury and lead at energies between 24.14 and 136 keV and for several rare earth elements at energies between 6.4 and 84.3

keV, with a view to evaluate the anomalous scattering factors. Budak *et al.* [18] have measured the total attenuation coefficient in the range $40 \leq Z \leq 52$ using ^{241}Am gamma rays.

Angelone *et al.* [19] have measured the mass attenuation coefficient for elemental materials in atomic range $6 \leq Z \leq 82$ using X-rays from 13 up to 50 keV. Alam *et al.* [20] have measured the linear and mass attenuation coefficients of different types of soil, sand, building materials and heavy beach mineral samples from the Chittagong and Cox's Bazar area of Bangladesh. Cross sections for total atomic attenuation, total atomic photoelectric and total atomic scattering in nine elements $58 \leq Z \leq 68$ at 59.537 keV are also reported by Karabult [21].

Midgley has measured the X-ray linear attenuation coefficient for materials containing elements hydrogen to calcium [22]. As it is inconvenient to use elements like hydrogen, carbon and oxygen in pure forms for measurement of their gamma mass attenuation coefficients, the measurements are to be done indirectly, by using compounds of the elements or a mixture of them. Teli *et al* [23] gave a simple method of measuring the total mass attenuation coefficients (μ/ρ) of the elements in a compound simultaneously and in a single experiment through the measurements of the (μ/ρ) values of the concerned compounds and using the mixture rule. The method is applied for the measurement of (μ/ρ) of hydrogen, carbon and oxygen by using acetone, ethanol and 1-propanol.

A simple relation between the total photoeffect cross section of an element and the total attenuation cross section of its compound has been derived by Umesh *et al* [24]. Total attenuation cross sections of some 15 simple compounds have been measured by performing transmission experiments in a good geometry set up. Using these values, they have determined total photoeffect cross sections of elements of $Z \geq 47$ at 514.0, 661.6, 1115.5, 1173.2 and 1332.5 keV gamma ray energies and compared with Scofield's theoretical cross sections. Accurate measurements on total attenuation coefficients for gamma rays was utilised by Govinda Nayak *et al* [25] to find effective atomic numbers (Z_{eff}) for the photoelectric process at 59.54 keV of three polymers, an alloy, a compound and an

element.

2.3.2 Using secondary X-rays excited from elemental targets by photons from radioactive sources

The second technique for obtaining the energies around the absorption edge is by secondary excitation of X-rays from targets using primary photons from radioactive sources. In this method, the incident photons excite the inner shells of the secondary excitation target and the subsequent decay of the excited atom results in the emission of the characteristic X-rays. The same qualitative arguments mentioned for the first method are applicable also for this technique.

Several authors recently reported the mass attenuation coefficients of elements around K-edge in various low energy ranges using ^{241}Am source and different targets. The K-absorption edge of some rare earth elements have been investigated by Mallikarjuna *et al.* [26]. X-ray attenuation coefficients of Cu, In and Se at various energies in the range $11.9 - 37.3$ keV were investigated by Cevika *et al.* [27]. The mass attenuation coefficients of Ag, Cs, Ba and La in the region $25 - 40$ keV using energy dispersive X-ray flourescence (EDXRF) were measured by Polat *et al.* [28]. The same technique was adopted by Necati Kaya *et al.* [29] to find the K-shell absorption jump factors and jump ratios for Tm, Yb, Lu, Hf, Ta, W, Re and Os in the energy region $56 - 77$ keV. Turgut *et al.* [14] have also determined the total mass attenuation coefficients for Co and some compounds of Co and Mn at different energies between 4.508 and 11.210 keV using secondary excitation method.

The total atomic attenuation,total atomic photoelectric and total atomic scattering cross sections by measuring the transmission factor has been fairly accurately calculated by Budak *et al* [18]. K X-ray fluorescence (XRF) spectra were also measured for Zr, Nb, Mo, Ag, In, Sn and Te at excitation energy of 59.54 keV. The method of secondary excitation has been used by Midgley *et al.* and Turgut *et al.* [30] to find the total mass attenuation coefficients for element Fe and compounds FeF_3, Fe_2O_3, $FeCl_2.4H_2O$, $FeCl_3.2NH_4Cl.H_2O$ at different en-

ergies in the 4.508-17.443 keV range. 59.5 keV gamma rays emitted from an ^{241}Am annular source was used to excite secondary exciters of Ti, V, Cr, Ni, Cu, Zn, As, Se, Br, Rb, Sr, Y, Zr, Nb and Mo. They have observed that mixture rule method is not a suitable method for determination of the mass attenuation coefficients of compounds, especially at energy that is near the absorption edge.

Ug ur Cevika *et al* [27] has measured the X-rays attenuation coefficients for Cu, In and Se in elemental state and the semiconductor $CuInSe_2$ at 15 different energies from 11.9 to 37.3 keV by using the secondary excitation method. Monochromatic photons were obtained using the secondary targets: Br, Sr, Mo, Cd, Te and Ba. 59.54 keV gamma rays emitted from an annular ^{241}Am radioactive source were used to excite secondary X-rays from these targets. Polat *et al* [28] have derived the K-shell absorption jump factors from mass attenuation coefficients measured using energy dispersive X-ray fluorescence for samples in the form of the compounds Ag_2O_3, $CsHCO_3$, $Ba(OH)_2$ and La_2O_3. These measurements, in the region 25-40 keV, were done in a transmission geometry utilizing the K X-rays from different secondary targets Sb, Pr, Nd and Sm excited by the 59.5 keV photons from an ^{241}Am annular primary source.

Necati Kaya *et al.* [29] have derived the K-shell absorption jump factors and jump ratios from new mass attenuation coefficient data measured using an energy dispersive X-ray fluorescence (EDXRF) spectrometer for Tm, Yb elements using Tm_2O_3, Yb_2O_3 compounds and pure Lu, Hf, Ta, W, Re and Os. The measurements, in the region 56 - 77 keV, were done in a transmission geometry utilizing the $K_{\alpha 1}$, $K_{\alpha 2}$, $K_{\beta 1}$ and $K_{\beta 2}$ X-rays from different secondary targets Yb, Ta, Os, W, Re and Ir, etc. excited by the 123.6 keV photons from an ^{57}Co annular source.

Gowda and Powers [31] used K_α and L_α X-ray lines produced by heavy ion interaction with thick targets of different materials as the source. Gopal and Sanjeeviah [32] have demonstrated the effect of multiple scattering for μt varying up to 4.2 for 84 and 661.6 keV gamma rays using carbon and lead absorbers. In their experiment using sodium iodide detector, they observed a deterioration of

the resolution of the detector as the absorber thickness increases above $1/\mu$, with a simultaneous increase in the value of the measured attenuation coefficient.

2.3.3 Using secondary X-rays excited from elemental targets by the Proton Induced X-ray Emission (PIXE) Technique

Proton Induced X-ray Emission (PIXE) is another versatile method [33] which utilizes the secondary excitation from targets. Here, protons are used instead of photons for secondary X-ray production. Rapid advances made in the analytical methods using X-rays make it possible for accurate measurements of values of X-ray attenuation coefficients which give important information about the composition of materials.

The technique has two definite advantages over the photon induced X-ray production method. First of all, the incident flux of protons (accelerated in a particle accelerator) is much larger than the number of incident photons available from radioactive sources. Consequently, the flux of secondary X-rays will be much larger and the statistical accuracy is correspondingly increased. Also, the background is relatively less in the PIXE spectrum. However, reported investigations on X-ray interactions using the PIXE technique are rather limited.

Varier *et al.* [34] have reported attenuation coefficients of copper, tantalum and lead targets using the technique of PIXE in the energy region $7 - 15$ keV. Pansky *et al.* [35] have used a new technique for studying Fano factor and the mean energy per ion pair in gases using low energy X-rays generated by the PIXE technique. A different method for measuring the thickness of aluminum foils used as X-ray absorbers in thick-target PIXE analysis using the change in K_β/K_α X-ray intensity is described by Campbell *et al.* [36]. Braziewicz *et al.* [37]have parameterized mass attenuation coefficients using a simple analytical representation of all elements between hydrogen and plutonium. Karydas [38] have carried out measurements on Resonant Raman Spectroscopy (RRS) using

vanadium K_α X-rays. Under favourable conditions, the PIXE method of X-ray production is superior to the photon induced X-ray generation as a source of the X-radiations for the interaction studies. This is so, especially because of the comparatively lower background in the PIXE spectra.

2.4 Methods involving continuously variable energy radiations

2.4.1 By Compton scattering from a suitable target

All the three techniques mentioned above suffer from one common disadvantage, namely, that the available gamma energies are discrete. Continuously variable energy can be made available by the use of Compton scattering of the primary photons from radioactive sources. It is known that the energy of the Compton scattered photons depends both on the energy of the primary photons and on the angle of scattering. In a practical situation the scattered energy can be easily varied over a reasonably large range by varying the angle of scattering in the range from about 30^0 to 160^0. For example, in the case of 59.54 keV gamma rays from ^{241}Am source, the available Compton energies cover the range from 48.56 keV to 58.62 keV. However, the Compton scattering method also requires strong primary photon sources. Also, the scattered radiation will not be strictly monochromatic : it is subject to an energy spread decided by the spread in the scattering angles arising from finite dimensions of the source and target. Budak and Polat [39] and Polat *et al.* [40] have applied this technique for the measurement of the K-shell absorption jump factors and jump ratios in some rare earth elements (Gd, Dy, Ho and Er)in the energy range $48 - 59$ keV from attenuation measurements near the absorption edge energies. They have used Aluminium as the secondary exciter.

2.4.2 Using Parametric X-ray Emission technique

An entirely new technique was developed recently by Tamura *et al.* [41] to measure mass attenuation coefficients around the K-edge for elements Zr, Nb and Mo. Their technique involves the emission of X-rays around the Bragg angle when relativistic electrons are incident on a crystal plate like silicon. This process has been called the Parametric X-ray Radiation (PXR). The X-rays generated by this technique are highly monochromatic, have continuously variable energy and are directed and coherent.

2.4.3 Tunable X-ray source

Yet another method, recently utilized for attenuation measurements is using tunable X-ray sources. The X-ray attenuation coefficients of bismuth and of uranium were measured in the regions of 40 - 240 and 70 - 240 keV, respectively, using a tuneable hard X-ray source based on the linear electron accelerator at the University of Ghent by Maternaa *et al* [42]. A low energy range (120 keV) tunable monochromatic X-ray source for metrological studies is described by Marie-Christine *et al* [43]. They have used the set-up to find the attenuation coefficients in the 410 keV energy range. The results for aluminum and copper with average relative uncertainties of 1% and 3% respectively.

2.5 Multiple scattering effects and the criterion $(\mu t \leq 1)$

In general, for experiments aimed at the determination of attenuation coefficients, the total absorber thickness used is less than one mean free path (given by $1/\mu$). This is referred to as the $\mu t \leq 1$ criterion. It is used to ensure that multiple scattering effects are negligible. Gopal and Sanjeeviah [32] have demonstrated the effect of multiple scattering for t varying up to 4.2 for 84 and 661.6 keV gamma rays using carbon and lead absorbers. In their experiment using sodium

iodide detector, they observed a deterioration of the resolution of the detector as the absorber thickness increases above $(1/\mu)$, with a simultaneous increase in the value of the measured attenuation coefficient. Therefore Gopal and Sanjeeviah had stressed this criterion in their work with 84 and 661.6 keV gamma rays using carbon and lead absorbers.

The effect of multiple scattering on the pulse height distribution of the transmitted gamma rays and on the measured attenuation coefficients was studied and shown to be small up to three mean free paths by Kane *et al* [44]. Values of attenuation coefficients were determined in the case of lead for 0.662 MeV, 1.116 MeV, 1.17 MeV and 1.33 MeV gamma rays, and in the case of tantalum and molybdenum for 0.662 MeV and 1.116 MeV gamma rays.

Varier and Kunju [45] conducted a study of the effect of transverse dimensions, that is, in a direction perpendicular to the direction of the incident beam. They concluded that for small transverse dimensions, absorber thickness up to even four mean paths does not significantly contribute to multiple scattering. For larger transverse dimensions, multiple scattering is important and could affect the measured attenuation coefficient for absorber thickness above one mean free path. The criterion ($\mu t \leq 1$) could also apply for transverse dimensions also.

2.6 Studies specifically focussed on absorption edges

If the photon energy is high enough, the photoabsorption spectrum comprises the characteristic edges (K, L, M etc.,) corresponding to the binding energies at which absorption coefficient jumps to higher values. Photon attenuation measurements around the edges gain importance because of this phenomena and there have been several attempts to make the measurements around these edges, especially around K-edge.

Near K-edge linear attenuation coefficients for stoichiometric crystalline and amorphous gallium arsenide were derived from total electron yield photocurrent

measurements by Owens *et al.* [46]. Their measurements show considerable near-edge structure when compared to curves generated from standard atomic data tables. However, very little difference is found between the crystalline and amorphous samples, suggesting that the bulk of the structure arises from the local coordination environment. Mallikarjuna *et al.* [26] have measured the total attenuation cross sections of rare-earth elements in a narrow beam good geometry using a high-resolution hyper pure germanium detector in the energy range $6 - 85$ keV. The data have been used to derive the K-shell photoeffect cross sections at the K-edge, the oscillator strength and the K-jump ratio of the elements La, Ce, Pr, Nd, Sm, Gd, Dy, Ho and Er.

The K-shell fluorescence yield, fluorescence cross-section and ratio between the radiative transition width and the Auger transition width have been measured for medium-Z elements, $30 \leq Z \leq 50$, using a geometrical configuration method by Gudennavar [47]. They have also measured the K-shell fluorescence cross section or K X-ray production cross section, the K-shell fluorescence yield, and the ratio between the widths of the radiative transition and the Auger transition, for some high-Z elements $62 \leq Z \leq 82$ [48].

Murty *et al.* [49] have determined total photon cross sections around the K edges of four elements Cu, Sn, Pb and U using a Ge(Li) detector, and argon and krypton proportional counters on a 'good geometry' set-up. The total photoelectric cross sections are extracted by subtracting the small scattering contribution from the total photon cross sections. They have also evaluated total-to-K-shell photoelectric cross section ratios (K-jump ratios) by extrapolating the total photon cross section data to the K-edge.

Photoelectric interaction below the K edge were studied by Reddy *et al.* [50] using the transmission method in the heavy elements U, Th, Pb, and Au at energies 30.9, 35.9, and 55.4 keV. The photoelectric cross sections, obtained by subtracting the small scattering contributions from the total cross section, are compared with theoretical predictions of Scofield [51] and of Storm and Israel [1]. General agreement is obtained, except for U and Th at 30.9 keV where their

experimental values show a slight preference to the calculations of Storm and Israel rather than the theoretical ones used by Scofield.

2.7 Studies related to mixture rule

In the description of photon attenuation by mixtures of elements, it is a standard practice to assume that the contribution of each element to the attenuation is additive. This assumption yields the well-known mixture rule [52]which gives the attenuation coefficient of any substance as the sum of the appropriately weighted contributions from the individual atoms. The mixture rule is valid when the effects on the atomic wave function of molecular bonding and chemical or crystalline environment are negligible. These values are also believed to be affected by the chemical, molecular and thermal environments. This is because of the existence of fine structure above the edge. These phenomena lead to the deviation of the experimental (μ/ρ) values from that of the theoretical values, since the calculation of the theoretical value has been done by considering the cross-section for an isolated atom. This deviation is termed as the breakdown or the non-validity of the mixture rule.

Turgut *et al* [30] have studied X-ray attenuation coefficients at different energies and the validity of the mixture rule for the elements Co, Mn, and compounds Co_2O_2, $CoCl_3.6H_2O$, $CoSO_4.7H_2O$, $MnCO_3$, $KmnO_4$, $MnCl_2.2H_2O$, $MnCl_2.4H_2O$ at different energies between 4.508 and 11.210 keV using a secondary excitation method. Ti, Co, Ni, Cu, Zn, As, Se were chosen as secondary exciter. Gamma rays (59.54 keV) emitted from an ^{241}Am annular source were used to excite a secondary exciter. They have shown that for a given incident photon energy the mixture rule breaks down not only for the compounds which contain an element whose K-edge energy is less than the photon energy, by as much as approximately 1500 eV, but also for those for those with K-edge energy slightly more than the photon energy by approximately 100 eV. In other words, the mixture rule breaks down for photon energies ranging from about 100 eV below the K-edge to about

1500 eV above K-edge.

Very few measurements have been made on the non-validity of the mixture rule. In the case of measurements near the bromine K-edge, the results showed that the mixture rule breaks down for incident photon energies within 1 keV above the edge [53, 54]. Jackson [55] pointed out that the range of validity of the mixture rule is not established close to the absorption edge. Nagel [56] had also pointed out, while discussing the absorption edge effects in electron probe microanalysis, that the tabulated values can be in error by 50% near an edge and by 10% up to 400 eV above the edge. Hubbell *et al.* [57] estimated the magnitude of the discrepancy between theoretical and experimental K-edge cross-sections for the elements from Ti to Zn to be in the range from 3% to 12%. However, Govinda Nayak [58] asserts that the mixture rule can be used with confidence to evaluate attenuation coefficients in polymers also, as in the case of compounds and alloys. Effective atomic numbers (Z_{eff}) of three polymers, an alloy, a compound and an element have been determined for photoelectric process at 59.54 keV from the accurately measured total attenuation coefficients, for γ ray attenuation. Possible conclusions are drawn on electron binding effects and K-edge effects.

A method to determine the K-shell photo effect cross sections of some compounds of the rare earth elements La, Ce, Pr, Nd, Sm, Gd, Dy, Ho and Er have been developed a new method, for energies above the K-edge of these elements, by Mallikarjuna *et al.* [26]. In this method, the K-shell photoeffect cross sections of rare earth elements at energies above the K-shell threshold are obtained by using log-log plot of the experimentally measured total attenuation cross sections of their simple compounds. The method does not require any knowledge of the contributions of other competing processes. A simple formula has been obtained by studying the variation of the K-shell photoeffect cross sections versus E and Z. This formula provides for an easy and rapid evaluation of the K-shell photoeffect cross sections for any element with $57 \leq Z \leq 68$ and for energies up to 84.3 keV.

2.8 Studies on anomalous scattering factors

The anomalous scattering factor (ASF) of X-ray resonant scattering changes remarkably near an absorption edge of an atom. It is well known that this change is significant for the phase determination of crystal structure factor and the study of X-ray magnetic scattering. ASF ($f^{'} + if^{"}$), near the absorption edge is so sensitive to the conduction band structure and the lifetime of intermediate transition process that it is not easy to evaluate it theoretically. Thus, it is interesting to investigate the consistency between the calculated ASF and the measured one. This process has been extensively studied theoretically as well as experimentally in view of its importance in some nuclear-physics, radiation-shielding, and astrophysical problems.

Chantler [59] addresses key discrepancies and derives theoretical results in near-edge soft X-ray regions. Reliable knowledge of the complex X-ray form factor and the photoelectric attenuation coefficient is required for crystallography, medical diagnosis, radiation safety and XAFS studies. This work brings out new theoretical investigation in resolving discrepancies of atomic form factors and attenuation coefficients in the near-edge soft X-ray regime . Cromer and Liberman [60] have given extensive tabulations of dispersion corrections over a range of wavelengths commonly used by crystallographers. Kissel *et al* [61] have developed a computer program based on the second order S-matrix formalism to predict the total atom Rayleigh scattering amplitudes. Kissel and Pratt [63] have tabulated the values of the high-energy limit, based on the S-matrix calculations, to be added to $f^{'}$ and also given the values of correction to be added to the CromerLiberman $f^{'}$ values. Bin Zhoua *et al* [62] proposes simple computational schemes to calculate the anomalous scattering factors g' and g" for ions, which utilize only the subshell photoionization cross sections of neutral atoms and ionic edge positions, without any ionic photoionization cross sections. Recently, Cullen *et al* [64] have provided a photon data library (EPDL97) that includes photon interaction data for all elements with atomic number between 1 and 100 over the range 1 eV to 100 GeV. D. V. Rao *et al*[65] measured the elastic scattering cross

sections for Pt, Au and Pb in the energy region $5.41 \leq E \leq 9.23$ keV. They have also developed a new method to estimate the degree of monochromaticity, geometrical effects of the measuring system, solid angle correction and some considerations which are necessary in experiments using X-ray tube with secondary target arrangement. Henke *et al* [66] have given tabulations of the dispersion corrections calculated for all Z in the energy range 30 eV to 30 keV, based on a semi-empirical approach using theoretical experimental attenuation coefficient data base.

On the experimental side, it can be noticed that two types of techniques have been mainly employed to determine the values of f' and f ". These are: (1) direct method and (2) attenuation coefficient method. Direct method has been employed by several investigators [67, 68, 69, 70] to calculate f' and f''. Appaji Gowda *et al* [17] derives the dispersion corrections to the forward Rayleigh scattering amplitudes of tantalum, mercury and lead derived using photon interaction cross sections. The same authors have also determined the anomolous scattering factors of some rare earth elements La, Ce, Pr, Nd, Sm, Gd, Dy, Ho and Er [16] for the energy region from 6 to 85 keV. They have used Scofield's [51] photoeffect cross-sections compiled in XCOM program, below 6 keV.

References

[1] E. Storm and H. I. Israel, *Nuclear Data Tables* **A7**, 565.

[2] J. H. Hubbell, *Int.J. Appl. Radiat. Isot.* **33**,1269 (1982).

[3] B. L. Henke, P. Lee, T. J. Tanaka and B. K. Fujikawa, *Atomic Data Nucl.Data Tables* **27**, 1 (1982).

[4] E. B. Saloman, J. H. Hubbell and J. H. Scofield, *Atom. Data Nucl. Data Tables* **38** 1 (1988).

[5] M. J. Berger and J. H. Hubbell, *XCOM: Photon Cross sections on a Personal Computer*", NBSIR 87 (1987).

[6] L. Gerward, N. Guilbert, K. Bjorn Jensen and H. Levring, *Radiat. Phys. Chem.* **60**,23 (2001).

[7] I. Orlic, I. Bogdanovib, Shijun Zhoua and J. L. Sancheza *Nucl.Instrum. Methods B*, **150**, 40 (1999).

[8] E. B. Saloman and J. H. Hubbell, *NBSIR* 86-3431 (1986).

[9] Wm. J. Veigele, *Atomic Data Tables* **5**, 51 (1973).

[10] J. Braziewicz, E. Braziewics and M. Pajek, *Nucl.Instrum. Methods***75** 68(1993).

[11] J. H. Hubbell, *Atomic Data and Nuclear Data Tables* **3**, 241 (1971).

[12] B. Roy, B. K. Chatterjee, S. C. Roy, N. Bhattacharya and N. Choudhury, *Applied Radiation and Isotopes*, **48**, 785 (1997).

[13] R. Preseren and A. Korde, *Radiation Physics and Chemistry*, **55**, 363 (1999).

[14] U. Turgut, A. Simsek, E. Buyukkasapp and M. Ertugrul, *Spectrochim Acta B* **57**, 261 (2002).

[15] N. Ramachandran, K. Karunakaran Nair, K. K. Abdullah and K. M. Varier, *Pramana J.Phys.* **67**, 507 (2006).

[16] S. B. Appaji Gowda, M. L. Mallikarjuna, R. Gowda and T. K. Umesh *Pramana J.Phys.* **61**, 539 (2003).

[17] S. B. Appaji Gowda, M. L. Mallikarjuna, R. Gowda and T. K. Umesh, *Nucl. Inst. and Methods in Phys. Res. B* **243**, 2 (2006).

[18] G. Budak, A. Karabulut, and M. Ertrulb, *Nucl. Inst. and Methods in Phys. Res. B* **149**, 379 (1999).

[19] M. Angelonea, T. Bubbab and A. Espositoc, *Appl. Rad. and Isotopes* **55**, 505 (2001).

[20] M. N. Alam, M. M. H. Miah, M. I.Chowdhury, M. Kamal, S. Ghose and R. Runi, *Appli. Radiat. Isotop.* **54**, 973 (2001).

[21] A. Karabult, A. Gurol, G. Budak and M. Eturgrul, *Nucl. Instrum. Methods B***227**, 485, **92**, 143 (2005).

[22] S. M. Midgley, *Radiation Physics and Chemistry* **72**, 525 (2005).

[23] M. T. Teli, R. Nathuram and C. S. Mahajana, *Radiation Measurements* **32**, 329 (2000).

[24] T. K. Umesh and C. Ranganathaiah, *Nucl.Instrum Methods B*: **5**, 472 (1984).

[25] N. G. Nayaka, M. G. Vijayaa and K. Siddappa *Rad. Physics and Chemistry* **61**, 559 (2001).

[26] M. L. Mallikarjuna, S. B. Appaji Gowda, K. E. Ganesh, R. Gowda and T. K. Umesh, *Nucl. Instrum. Methods B* **215**, 4 (2004).

[27] Ug ur Cevika, Hasan baltasb, A. Celika and E. Bacaksiza, *Nucl. Instrum. Methods B* **247**, 173 (2006).

[28] R. Polat, G. Budak, A. Gurol, A. Karabulut and M. Ertugurul, *Radiation Measurements* **39**, 409 (2005).

[29] N. Kaya, E. Tirasoglu, G. Apaydina, V. Aylikcia and E. Cengiza, *Nucl. Instrum. Methods B* **262**, 16(2007).

[30] U. Turgut, E. Buyukkasap, O. Simsek and M. Ertugrul, *Journal of Quant. Spectr. and Radiat. Transfer* **92**, 1365 143(2005).

[31] R. Gowda and D. Powers , *Phys. Rev. A* **32**, 2637 (1985).

[32] S. Gopal and B. Sanjeevaiah, *Nucl. Inst. Meth.* **107** , 221 (1973).

[33] S. A. E. Johansson and J. Campbell, *PIXE A Novel Technique for Elemental Analysis* John Wiley and Sons 713 (1988).

[34] K. M. Varier and M. P. Unnikrishnan, *Phys. Rev. A***33**, 2382 (1986).

[35] A. Pansky, A. Breskin and R. Chechik, *J. Applied Physics* **79**, 8892 (1996).

[36] J. L. Campbell, W. J. Teesdale and J. A. Maxwell, *Nucl. Instrum. Methods B* **43**, 197 (1989).

[37] J. Braziewicz, E. Braziewics and M. Pajek, *Nucl. Instr. and Methods in Physics Research B* **75** 68 (1993).

[38] A. G. Karydas and T. Paradellis, *J. of Phys. B - Atomic, Molecular and Optical Physics* **30**, 1893 (1997).

[39] G. Budak and R. Polat, *J. of Quant. Spectr. and Radiat Transfer* **88**, 525 (2004).

[40] R. Polat, O. Icelli and G. Budak, *Analytica Chimica Acta* **505**, 307 (2004).

[41] M. Tamura, T. Akimoto, Y. Aoki, J. Ikeda, K. Satoa, F. Fujita, A. Homma, T. Sawamura and M. Narita, *Nucl. Instrum. Methods A* **484**, 642(2002).

[42] Th. Maternaa, J. Jolie, W. Mondelaersb and B. Masschaeleb, *Radiat. Phys. Chem* **59** 449 (2000).

[43] M. C. Lpy, L. Ferreux and J. Plagnard, *Applied Radiation and Isotopes* **60** 159 (2004)

[44] P. P. Kane, G. Basavaraju and K. M. Varier *Nucl. Instr. and Methods in Phys. Research Section B* **149**, 379 (1999).

[45] K. M. Varier, S. Nasirudden Kunju and K . Madhusudanan, *Phys.Rev .A* **33** 2378 (1986).

[46] A. Owens, J. F. W. Mosselmans and A. Peacock, *Radiat. Phys. and Chem.* **66**, 1 (2003).

[47] S. B. Gudennavar, N. M. Badigernext term, S. R. Thontadarya and B. Hanumaiah, *Radiat. Phys. and Chem.* **68**,721 (2003).

[48] S. B. Gudennavar, N. M. Badiger, S. R. Thontadarya and B. Hanumaiah *Radiat. Phys. and Chem.* **68**, 745 (2003).

[49] V. R. K. Murty, K. S. Rao, K Parthasaradhi *et al J. Phys. B: At. Mol. Phys* **10**, 3189 (1977).

[50] D. K. S. Reddy, K. Premachand, V. Radha Krishna Murty, J. Rama Rao, and V. Lakshminarayana, *Phys. Rev. A* **13**, 326 (1976).

[51] J. H. Scofield, *Lawrence Livermore National Laboratory Report* UCRL-**51326**, (1973); personal communication of additional data 0.1 to 1.0 keV (1985).

[52] R. D. Evans, *The Atomic Nucleus*,(Tata McGrawHill), 714 (1955).

[53] V. Lakshminarayan , A. T. L. Tan , I. S. Giles and A. Rajaratnam, *Nuovo Cimento*, **91A**, 331 (1986).

[54] A. T. L. Tan, V. Lakshminarayan, I. S. Giles and A. Rajaratnam, *Nuovo Cimento*, **99A**, 587 (1988).

[55] D. F. Jackson, *Nuclear Instruments and Methods* **193**, 387 (1982).

[56] D. Nagel, *National Bureau of Standards*, 189 (1968) 1359.

[57] J. H. Hubbell, W. H. McMaster, Del Grande N. Kerr and J. H. Mallett *Int. Tables X-ray Crystallogr* 1974;4:47.

[58] N. Govinda Nayak, M. G. Vijaya and K. Siddappa, *Radiat. Physics and Chem.* **61**, 559 (2001).

[59] C. T. Chantler *Phys. Chem. Ref.* Data **24**, 71 (1995).

[60] T. Cromer and D. Liberman, *J. Chem. Phys.* **53**, 1891 (1970).

[61] L. Kissel, S. C. Roy and R. H. Pratt, *Phys. Rev. A* **22**, 1972 (1980).

[62] Bin Zhou, Lynn Kissel and R. H. Pratt, Nucl. Instrum. Methods **66**, 307 (1992).

[63] L. Kissel and R. H. Pratt, *Acta Crystallogr.* **A46**, 170 (1990).

[64] D. E. Cullen, E. Dermott, J. H. Hubbell and L. Kissel *The Evaluated Photon Data Library*, 97 Version (Lawrence Livermore National Laboratory, 1997).

[65] D. V. Rao, R. Cesareo and G. E. Gigante , App. Radiation and Isotopes **49**, 835 (1998).

[66] B. L. Henke, P. Lee, T. J. Tanaka, R. L. Shimambukuro and B. K. Fujikawa, *At. Data Nucl. Data Tables* **27**, 1 (1982) B. L. Henke, E. M. Gullikson and J. C. Davis, *At. Data Nucl. Data Tables* **54**, 181 (1993).

[67] P. Drier, P. Rabe, W. Malzfeldt and W. Niemann, *J. Phys.* **C17**, 3123 (1984).

[68] L. Gerward, G. Thuesen, S. Jensen and I. Alistrup, *Acta Crystallogr.* **A35**, 852 (1979).

[69] M. Keffi, J. M. Andre, Y. Heno, G. Gorgi and C. Bonnelle, *Phys. Rev.* **45**, 2859 (1992).

[70] J. H. Barkyoumb and D. Y. Smith, *Phys. Rev.* **41**, 4863 (1990).

Chapter 3

Attenuation studies using Compton scattered photons on Sm, Eu, Gd, Tb, Dy and Er around the K-edge

3.1 Introduction

Photon interaction studies at energies around the absorption edge have attracted the attention of researchers in the field for quite some time now [1, 2, 3, 4]. The abrupt jump in the photoelectric cross section across the edge has been of main interest for such studies. These investigations require a source of continuously variable energy photons to probe the energy region around the absorption edge. As already discussed in the previous chapter, Compton scattering offers a convenient and excellent technique for this purpose. Here the primary gamma rays from a radioactive source are Compton scattered from a secondary exciter target of aluminium. The energy of the Compton scattered gamma rays at an angle θ is given by

$$E = \frac{E_o}{\{1 + \alpha(1 - cos\theta)\}}, \tag{3.1}$$

where E_o is the incident gamma energy and α is the ratio of E_o to the rest mass energy of the electron. Thus the photon energy can be continuously varied from

a lower value to a maximum value depending on the practically allowed limits on the scattering angle θ. These allowed limits on the angle of scattering are decided, on the lower side, by the requirement that either the direct gamma rays from the source or forward scattered gamma rays from the shielding material etc. should not fall on the absorber. On the larger angle side, the shielding around the source should not obstruct the view of the detector from the absorber. The only drawback of this technique is that the Compton scattered radiation will not be completely monochromatic. There is bound to be a certain spread in the scattering angles arising out of the finite dimensions of the source, target and detector, which will be reflected as a spread in the energy of the scattered radiation. It was Polat *et al.* [5] who first reported use of this technique for measuring the gamma ray attenuation coefficients for the elements Gd, Dy, Ho and Er at several energies around their K-edges. These authors obtained good agreement between theory and experiment.

^{241}Am presents a very suitable gamma ray source for measurements around the K-edge absorption threshold region of the rare earth elements. Its gamma energy, 59.54 keV, lies in between the K-edges of the rare earth elements Thulium (59.39 keV) and Ytterbium (61.332 keV). Keeping this fact in mind, gamma ray interaction studies [6] had earlier been carried out in our laboratory using oxides of rare earth elements at a single energy of 59.54 keV. Extending this work, we have now carried out attenuation measurements at several energies near the K-absorption edges of the rare earth elements Sm, Eu, Gd, Tb, Dy and Er. The gamma rays of the appropriate energies have been obtained by the process of Compton scattering from an aluminium target at various angles. The theoretical range of energies available by this technique is seen to be from 48.287 keV upto 59.54 keV corresponding to angles of scattering between 180^0 and 0^0 respectively.

3.2 Experimental details

The experimental arrangement employed in the present investigations is shown schematically in Figure 3.1.

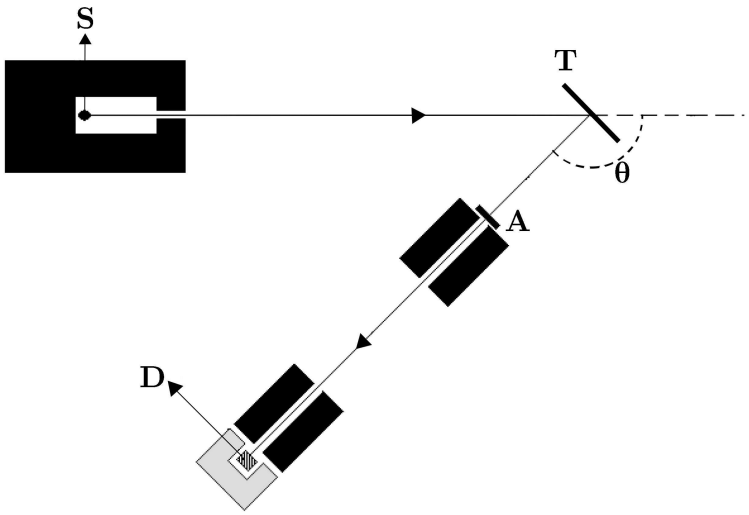

Figure 3.1: Schematic diagram of the experimental set up for narrow beam geometry gamma attenuation measurements.

The photograph of the setup is given in Figure 3.1.1

3.2.1 Source

The ^{241}Am source (S), procured from Amersham, England, had a strength of 300 mCi and was kept shielded with a 0.8 cm collimator in the front. It provided gamma rays of energy 59.54 keV for the present measurements. As already mentioned, in order to obtain variable energy gamma rays, the 59.54 keV photons from the source were Compton scattered from a secondary exciter target. For achieving this purpose, the source, along with the shielding, was fixed to a rotating arm mounted on a rigid aluminium circular table at a distance of 33 cm from the centre of rotation. The round table had angular graduations all around its circumference in order to facilitate accurate setting of the angle of scattering. The secondary exciter target (T) was an aluminium disc of thickness 1 cm. placed in a reflection geometry, at the centre of the rotating table with its plane making an angle equal to (π-θ)/2, θ being the scattering angle.

3.2.2 Absorbers

The absorbers (A) for the present measurements were prepared using oxides of rare earth elements Sm, Eu, Gd, Tb, Dy and Er. The absorbers were procured from various suppliers like Indian Rare Earths Limited, Alwaye, CSIR Lab, Thiruvananthapuram etc. The purity of the materials was ensured to be better than 99.5%. The absorbers were in the form of pellets of diameter 1.2 cm prepared using a pelletizer at a pressure of $10 - 12$ tonnes. In preparing the pellets, analar grade KBr was added as a binding agent. The effect of KBr on the measured attenuation coefficient was taken into account later on during the data analysis. The absorber was positioned in between the aluminium target and the detector so that the gamma rays transmitted through the target were detected in a narrow beam good geometry.

3.2.3 Detector and electronics

The scattered gamma rays from the aluminium target were detected by means of a well shielded HPGe GammaX detector (D) procured from ORTEC, USA. It had a resolution of 1.14 keV at 60 keV. A block diagram of the electronics setup is shown in Figure 3.2. An ORTEC 571 spectroscopy amplifier was used

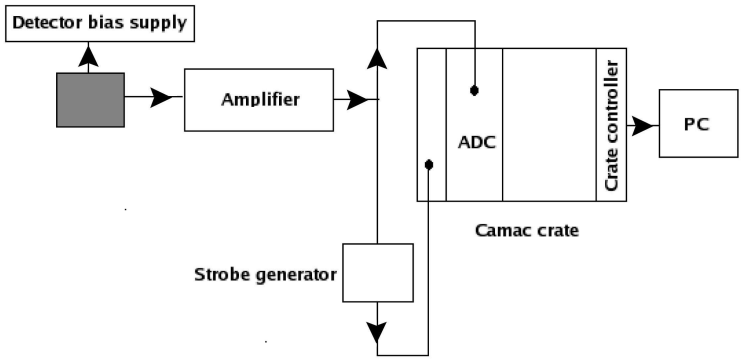

Figure 3.2: Electronic set up.

to properly shape and amplify the detector signals. The amplifier output pulses were then fed to a CAMAC based data acquisition and analysis system, consisting of a Kinetic CAMAC crate, crate controller, a 4k Quad ADC, supplied by the

Electronics Division, BARC and connected to a Personal Computer through a suitable interface card. A Linux based package, FREEDOM [7], developed at the Inter University Accelerator Centre (IUAC), New Delhi was used for the data collection and analysis. Details about this package are described in the next section. A photograph of the electronics set up used for processing and analysis of the detector pulses is shown in Figure 3.3.1. The figure shows the CAMAC crate (in the middle) housing the controller and ADC and the NIM module housing the amplifier and the Detector bias supply in the lower side.

3.2.4 FREEDOM Package

The FREEDOM software package for data acquisition as well as analysis normally has a Graphical User Interface (GUI) wherein the various functions are activated by mouse clicks on appropriate menu buttons. By mouse clicking on any of the buttons, a drop-down submenu appears. Further selection of the submenu items is again done by means of a mouse click. The GUI window of the package is shown in Figure 3.3.2. The spectra will be displayed in the central region of the GUI. The scales of the axes of the spectrum can be changed to our will by appropriate mouse functions on the horizontal and vertical scroll bars provided. Linear or Logarithmic scales can be chosen for the y axis. One can display either one dimensional spectra (1D) or two dimensional spectra (2D). A 1D spectrum will display the counts vs. channel number information. A 2D spectrum displays the correlation information between two 1D spectra. The two axes correspond to the channel numbers of the two 1D spectra and the counts information is displayed as different colours. Each colour will correspond to a certain range of counts. There is provision for data collection and analysis online and also for offline data analysis on already stored data. In the online mode, one loads the CAMAC configuration from a config file. This defines the various CAMAC functions to be used for the data acquisition, details about the hardware ADC, etc. The details about the various spectra to be generated online are then also loaded from a file. If an event wise data storage is required, the neces-

sary file should be opened. The same should be closed after the data collection is over. Otherwise, only the necessary spectra can be stored. Data collection can be started at any specific time and then stopped either manually, or after a preset time interval. If needed, the generated spectra can be saved either in text format or in binary format.

Analysis of the generated spectra will consist of spectrum fitting, retrieval of information about the centroids, peak areas, FWHMs, total counts within a chosen region of interest (defined by markers) etc. There is also provision for various manipulations like subtraction or addition of spectra, multiplication of spectra by a constant etc. These operations may be needed, for example, for background subtraction and for obtaining the total spectra for a long time period when the data are stored in separate runs of shorter intervals etc. In the offline mode, no CAMAC configuration is required. Only the information regarding the spectra need be loaded. In place of the data collection from the detector and associated electronics, now the data will be coming from the saved files. Apart from this all other functions are similar to those in the online mode.

3.2.5 Experimental procedure

Calibration of detector and electronics

Initially, the detector and the pulse processing electronics were calibrated using a 2.5 μC ^{241}Am source. The prominent gamma rays of energy 59.54 keV and the characteristic X-rays from the Neptunium daughter nucleus provided the necessary calibration energies. A typical pulse height spectrum of the source radiations is shown in Figure 3.3. The calibration curve has been plotted in Figure 3.4. It is seen that the calibration is quite linear in the energy region of interest.

In arranging the source and detector along with the shielding and the aluminium target at the centre on the experimental table with the angle graduations, care has been taken to ensure that the actual zero degree position coincides with

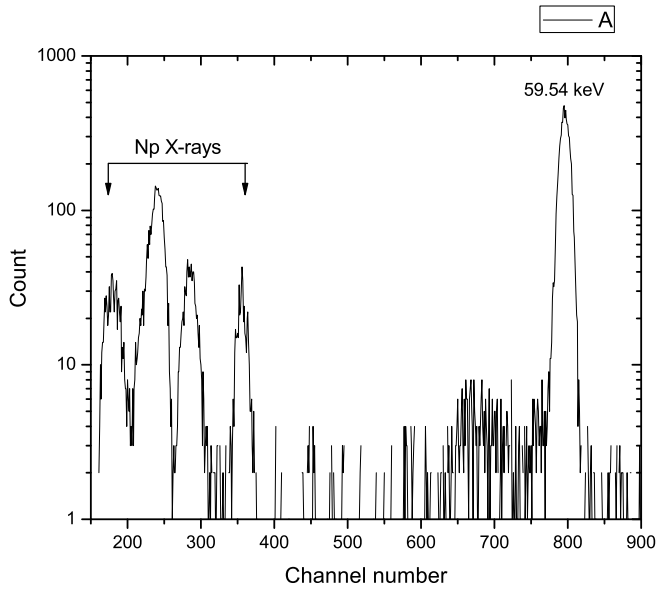

Figure 3.3: Typical spectrum of the radiations from the ^{241}Am source.

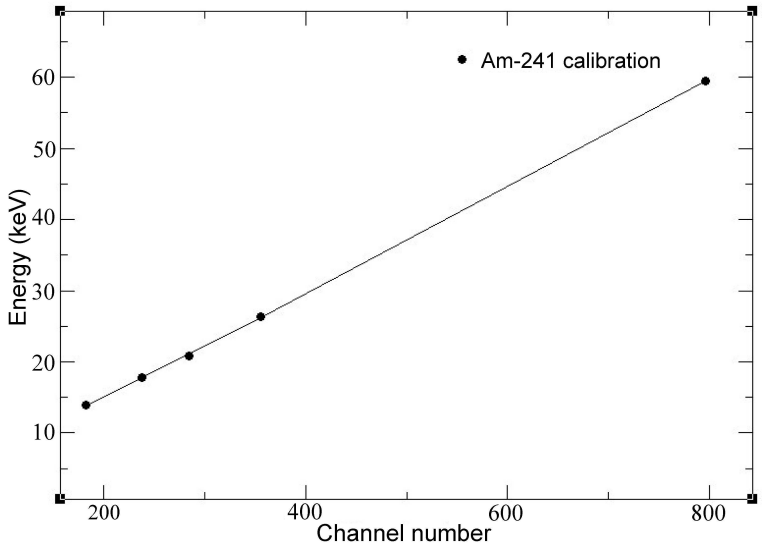

Figure 3.4: Calibration curve for the detector and electronics.

the zero on the table. To check this point and to apply any corrections if needed, the following procedure had been adopted.

First of all, the source along with its shielding, was positioned at several angles on either side around the zero degree direction. The direct gamma rays from the source were allowed to fall on the detector without the aluminium target in between. The number of detected photons were counted as a function of the angle of setting of the source. The plot of the counts vs. the angle setting is given in Figure 3.5. It is seen from the above plot that the set angle of *zero degree* is

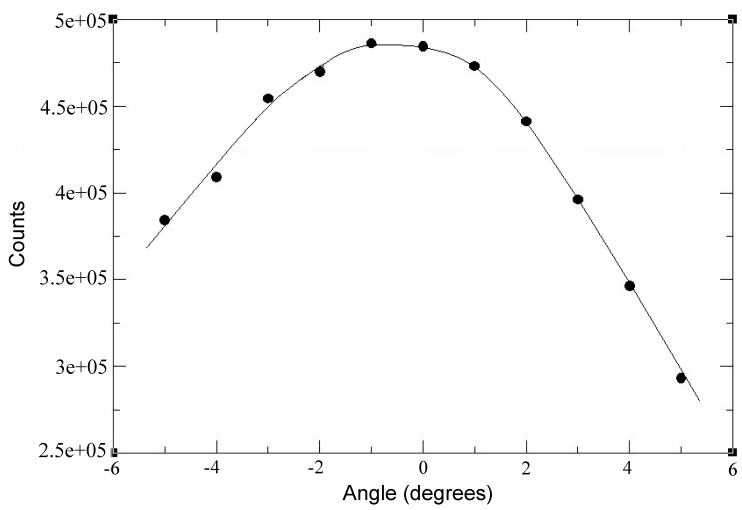

Figure 3.5: Data plot for determination of angle offset.

actually 0.7^0 off from the actual zero degree position. A correction to this effect was made for all the angle readings later on. The attenuation measurements comprised of first setting the angle of scattering for a specified scattered energy as given by eq.(3.1). The direct spectrum of the scattered radiation was then stored on the MCA for an interval of 30 minutes. The absorber was then positioned in between the aluminium target and the detector. The spectrum of the gamma rays transmitted through the absorber was stored for the same intervals of 30 minutes. Background spectra were also stored for the same time after removing first the secondary exciter and then the absorber. The background counts within the peak region of the scattered radiation was found to be the same, within statistical errors, in both cases.

Typical spectra of the ^{241}Am gamma rays Compton scattered at 80^o from the aluminium target, with and without a Dy pellet absorber are shown in the Figure 3.6. The mean energy of the scattered radiation, as calculated from eq.(3.1) is 54.31 keV. For reference, the expected spectrum in the photopeak region of monoenergetic radiations of the same energy is also shown superimposed in the same figure. The effect of the finite spread in the scattering angles is clearly seen. The effective spread in the scattering angles can be calculated by comparing the widths of the scattered spectrum and the photopeak of the monoenergetic radiations of the same mean energy and is seen to be about 0.36^o. The net counts

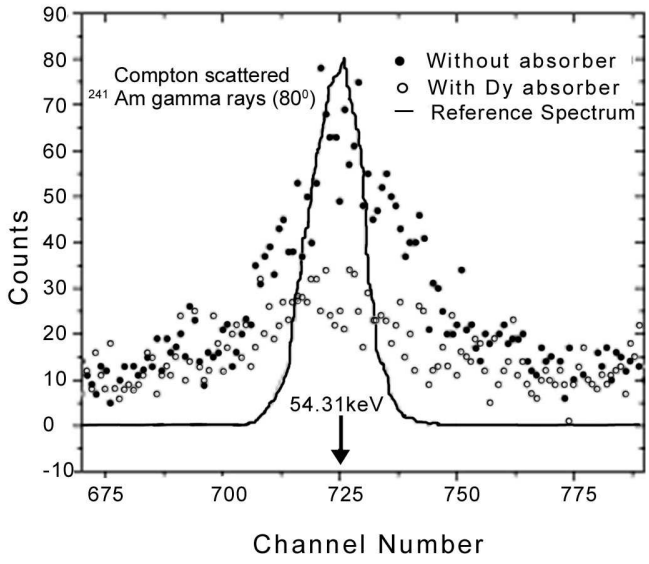

Figure 3.6: Comparison of spectra of Compton scattered radiations from an ^{241}Am source at 80^o with and without the pellet absorber (Dy) with that of monoenergetic gammas of energy 54.31 keV.

under the peak region of the scattered radiation from the aluminium target was extracted after subtraction of the background, with and without the absorber. Knowing the absorber thickness, the attenuation coefficient was calculated from the equation

$$I = I_0 exp[-(\mu/\rho)x.\rho], \tag{3.2}$$

where μ is the linear attenuation coefficient(cm^{-1}), ρ is the density of the sample (gcm^{-3}), x is the thickness of the absorber (cm), I_0 is the count value without

the sample and I is the count value of the radiation penetrating through the sample.

The above procedure was repeated for several energies to cover the K-edge, by varying the angular position of the source, thereby changing the scattering angle also. In the case of Sm and Eu, measurements could be made only on one side of the K-edge energy because of the obvious practical limitations on the scattering angle θ. In our geometry, the angular range which could be scanned was from 40^o to 140^o. This corresponds to an energy range from 49.38 keV to 57.96 keV. The K-edge energies of Sm and Eu are respectively 46.835 keV and 48.519 keV, which obviously are outside of the above range.

As already mentioned, at each setting of the angle of Compton scattering of the primary gamma rays, there is a certain spread in the scattering angles, decided by the finite dimensions of the absorber and detector. Consequently the attenuation coefficients derived from the observed spectra are really values averaged over the unavoidable energy spread and will not correspond to the attenuation coefficient values for the discrete energy of the scattered photons at that scattering angle. In order to extract the attenuation coefficients at the mean energy, we have adopted the following iterative procedure.

First of all we assume reasonable starting values for the attenuation coefficients at several equally spaced energy values covering the total spread in the scattered energies for the particular scattering angle chosen. Obviously the best set of starting values would be the XCOM values [9, 10] themselves (See below). These are treated as parameters in a least squares fitting programme. An effective attenuation coefficient for the non-monochromatic Compton scattered radiation is then evaluated as an average over the various possible scattering angles in the set up used. These values are compared then with the experimental values. The assumed values of the attenuation coefficients are then varied and an optimum set is arrived at using the least squares method. The value of χ^2 is then evaluated using the equation

$$\chi^2 = \sum_{i=1}^{N} [(\mu/\rho)_i - (\mu/\rho)_{fit,i}]^2, \tag{3.3}$$

where $(\mu/\rho)_i$ is the mass attenuation coefficient for i^{th} mean energy point calculated as an average over the angles, and $(\mu/\rho)_{fit,i}$ the current fitted value at the mean energy. The parameters are varied until χ^2 is minimized. In Appendix I, a flow chart for the computer program used to carry out the above least square fitting is presented.

The mass attenuation coefficients measured by the above iterative method correspond to the mixtures of the rare earth oxides with Potassium Bromide. In order to extract the mass attenuation coefficients of the rare earth elements, it is first necessary to know the coefficients KBr. The values of the mass attenuation coefficients were separately measured for KBr using pure KBr pellets. Using these additional data, the mixture rule [8] was used to extract the mass attenuation coefficients of the rare earth oxides. The rule gives the effective mass attenuation coefficient of any composite substance as the sum of the appropriately weighted contributions from the individual atoms. Thus, the mass attenuation coefficient is given by

$$(\mu/\rho) = \sum_i w_i(\mu/\rho)_i \tag{3.4}$$

where w_i is the proportion by weight, μ is linear attenuation coefficient in cm^{-1}, ρ (g/cm^3) is the density of the element and $(\mu/\rho)_i$ (cm^2/g) is the mass attenuation coefficient of the constituent element i of the compound. Theoretical values of the coefficients for oxygen required for extracting the values of the coefficients for the rare earth elements were obtained from the XCOM package [9, 10]. This package is a computer programme and data base, developed by Berger and Hubbell, which can be used to calculate, using a Personal Computer, theoretical photon cross sections for scattering, photoelectric absorbtion and pair production, as well as total attenuation coefficients, in any element, compound or mixture, at energies from 1 keV to 100 GeV. It utilizes a vast data base for all elements from hydrogen to fermium.

3.3 Results and discussion

First of all, the present results for the attenuation coefficients at selected scattering angles for the KBr pellets is given in Table3.1. The average values over the spread in the scattering angles are given in the second column of the table. The third column gives the values extracted at the energy corresponding to the mean scattering angle, extracted by the iterative procedure outlined above. These latter values are compared with the corresponding theoretical values obtained from the XCOM package. It is seen that there is reasonably good agreement between theory and experiment, within the uncertainties quoted in the table. In

Table 3.1: Comparison of present attenuation coefficient values for KBr with XCOM values

Photon energy (keV)	$(\mu/\rho)(Present)$ (cm^2/gm) (Average over angular spread)	$(\mu/\rho)(Present)$ (cm^2/gm) (Extracted value at the mean energy)	(μ/ρ) XCOM (cm^2/gm)
49.433	1.928± 0.241	2.655±0.332	3.248
49.974	2.057± 0.252	2.832±0.347	3.152
50.682	1.972 ±0.272	2.716±0.375	3.034
51.489	1.853 ±0.286	2.552±0.394	2.906
52.377	1.942 ±0.300	2.675±0.413	2.773
53.327	2.047 ±0.299	2.819±0.412	2.647
55.300	2.076 ±0.258	2.859±0.355	2.393

table (3.2)are given the experimental average (μ/ρ) values at the mean angles along with the fitted values obtained after χ^2 minimization. There is reasonably good agreement between these two values. As a representative of the results for the average attenuation coefficient values obtained in the present studies for the rare earth compounds we present in Figure 3.7 the results for the mixture of dysprosium oxide and potassium bromide.

In Figure 3.7, experimental values of (μ/ρ) represented by the solid circles are the raw data obtained from the spectra with and without the mixture absorbers. The XCOM values averaged over the spread in scattering angles are represented by the solid line. The extracted values of the attenuation coefficient for the

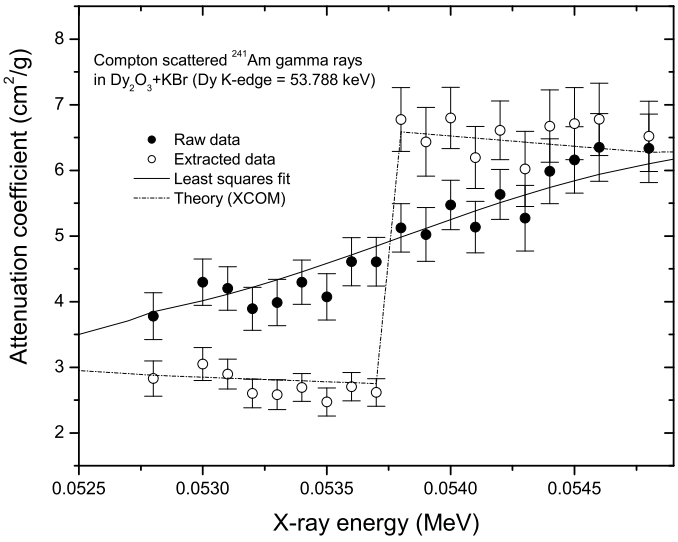

Figure 3.7: Variation of the attenuation coefficient with energy for a mixture of Dysprosium oxide and Potassium Bromide

mixture at the discrete energies corresponding to the different scattering angles are indicated by the open circles and the corresponding theoretical XCOM values by the dotted line. It is seen that there is reasonably good agreement between theory and experiment for the two sets of values. The errors on the experimental values are statistical ones. The K-edge energy for Dy is 53.788 keV. It may be noted that below the K-edge, the raw data are larger than the theoretical XCOM data represented by the dotted line, whereas above the K-edge, the raw data are smaller than the XCOM values. This is obviously due to the spread in scattering angles. The effect is dominant at the K-edge as obvious from the plot. As the energy of the incident radiation moves away from the K-edge on either side, the raw data approach the dotted line as expected. In Tables 3.2 - 3.4, the attenuation values derived from the present results for the six elements studied are presented along with the XCOM values. It is seen that the present experimental results tally more or less reasonably with the theoretical values, within experimental errors. In Figure 3.8 the attenuation coefficient values derived from the experimental results for the element Dy (as extracted by the procedure given in the previous section) are shown. Also given by means

of the solid line are the corresponding XCOM values. We can see an overall agreement between theory and experiment. Similar plots for the elements Gd, Tb and Er are shown in Figures 3.9, 3.10 and 3.11. In these cases also, we see a general agreement between theory and experiment, within the experimental uncertainties. The clear jump in the attenuation coefficient values around K-edge energies are quiet evident from the plots.

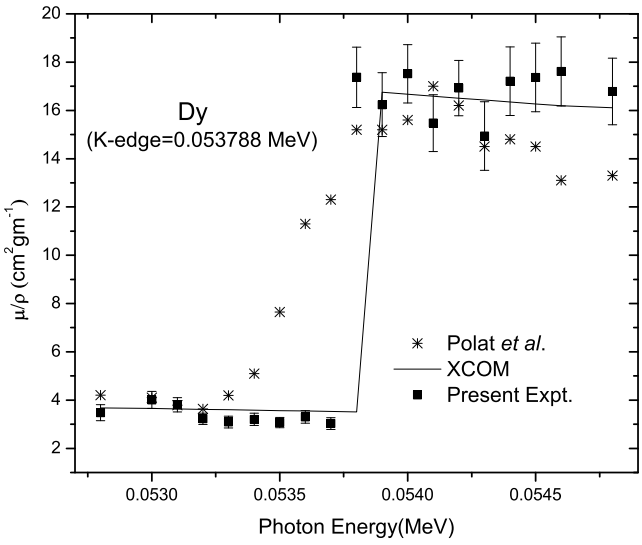

Figure 3.8: Comparison of the attenuation coefficients for Dy with XCOM values

In Figures 3.8 to 3.11 we have shown by the cross marks some representative experimental results of Polat *et al.* [5] for the elements Dy, Gd, Tb and Er respectively in the energy range of our present measurements. It is obvious from the plots that our results are in closer agreement with theory than those of Polat *et al.* A comparison of the plots of their results with Figure 3.7 suggests that probably the results of Polat *et al.* are the averaged values over the relevant spread in scattering angles in their set up. No mention of this effect has been made by these authors in their paper. Probably if due account of the effect had been taken by the authors, their results would have been in closer agreement with the theoretical XCOM values as observed in our case. In Figures 3.12 and 3.13 we present the comparison of the experimental attenuation coefficient

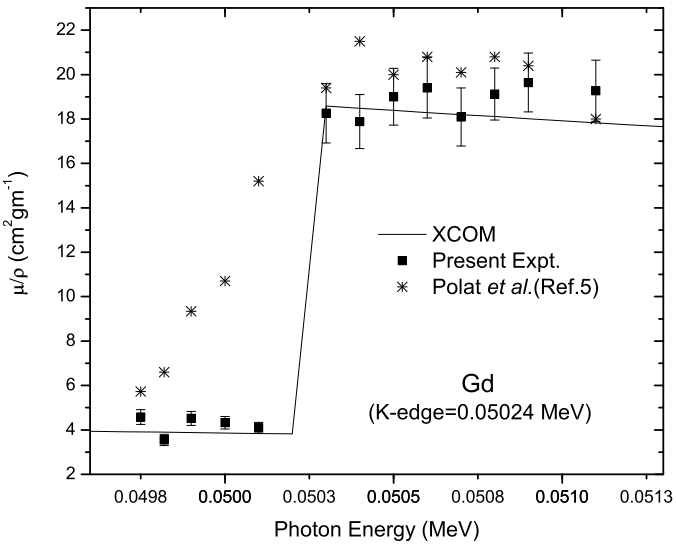

Figure 3.9: Comparison of the attenuation coefficients for Gd with XCOM values

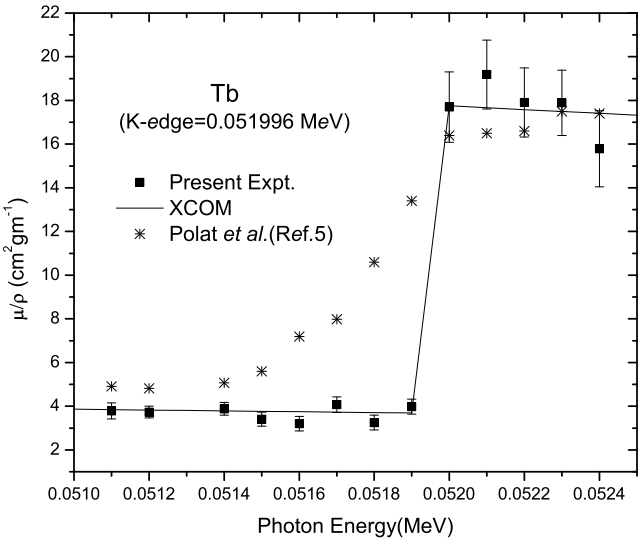

Figure 3.10: Comparison of the attenuation coefficients for Tb with XCOM values

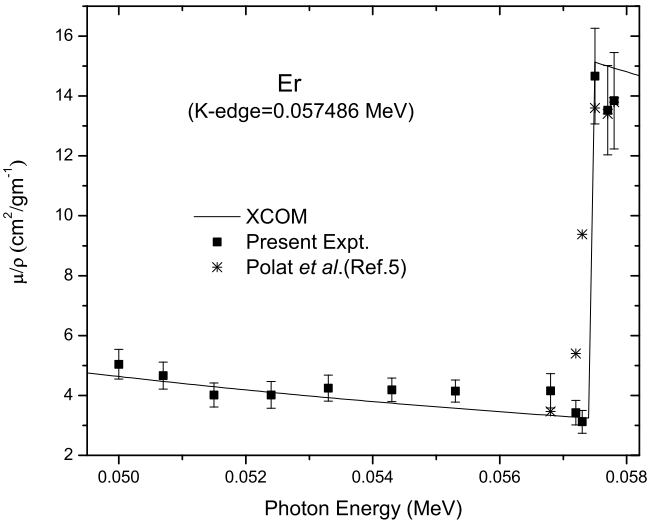

Figure 3.11: Comparison of the attenuation coefficients for Er with XCOM values

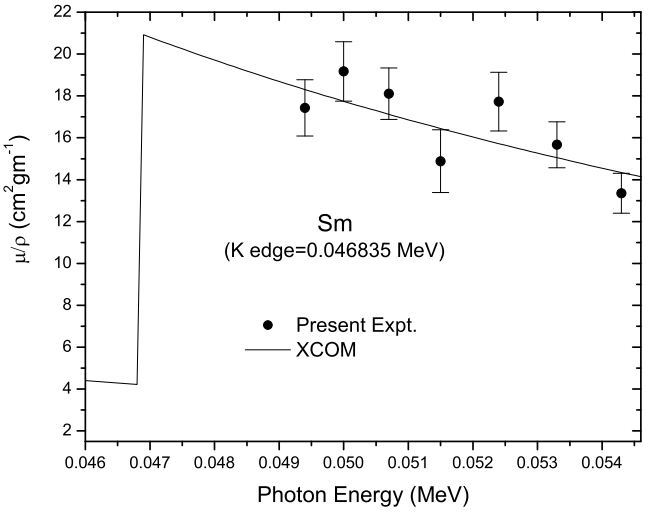

Figure 3.12: Comparison of the attenuation coefficients for Sm with XCOM values

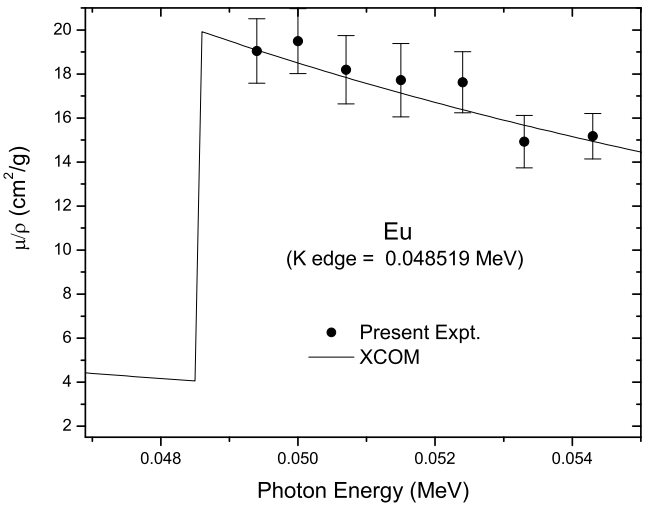

Figure 3.13: Comparison of the attenuation coefficients for Eu with XCOM values

values for the other rare earth elements investigated, namely, Sm and Eu. As already mentioned, for these two elements we have data only above the K-edge, for the obvious practical limitations on the scattering angle. We see that for these elements also, the agreement with theory is reasonably good.

In all the cases extracted, experimental values for the attenuation coefficients are seen to be consistent with the theoretical XCOM values within the quoted uncertainties. At the near K-edge energies investigated, our results do not indicate any breakdown of the mixture rule. The agreement with theory proves the reliability of the present method of extraction of the attenuation coefficients for the pellets at the discrete energies from the raw values, averaged over the spread in the energies.

Table 3.2: Comparison of measured values of attenuation coefficients for Dy and Er with XCOM values.

Dy			Er		
Photon energy (MeV)	Present Expt. $(\mu/\rho)(cm^2/gm)$	XCOM	Photon energy (MeV)	Present Expt. $(\mu/\rho)(cm^2/gm)$	XCOM
0.0528	03.48±0.33	03.67	0.0500	05.04 ± 0.49	04.63
0.0530	04.00±0.35	03.64	0.0507	04.66 ± 0.45	04.47
0.0531	03.80±0.30	03.62	0.0515	04.02 ± 0.40	04.29
0.0532	03.23±0.24	03.60	0.0524	04.02 ± 0.44	04.10
0.0533	03.09±0.25	03.58	0.0533	04.24 ± 0.43	03.93
0.0534	03.20±0.25	03.57	0.0543	04.19 ± 0.39	03.74
0.0535	03.07±0.21	03.55	0.0553	04.15 ± 0.37	03.57
0.0536	03.30±0.26	03.53	0.0568	04.15 ± 0.57	03.33
0.0537	03.03±0.24	03.51	0.0572	03.43 ± 0.41	03.27
0.0538	17.37±1.25	16.75	0.0573	03.12 ± 0.38	03.26
0.0539	16.24±1.32	16.67	0.0575	14.66 ± 1.60	15.13
0.0540	17.52±1.21	16.59	0.0577	13.53 ± 1.49	15.00
0.0541	15.47±1.18	16.51	0.0578	13.84 ± 1.61	14.93
0.0542	16.92±1.14	16.43			
0.0543	14.94±1.42	16.35			
0.0544	17.21±1.42	16.27			
0.0545	17.37±1.42	16.19			
0.0546	17.62±1.43	16.11			
0.0548	16.79±1.38	15.96			

Table 3.3: Comparison of measured values of attenuation coefficients for Sm and Eu with XCOM values.

Photon energy (MeV)	Present Expt. $(\mu/\rho)(cm^2/gm)$	XCOM	Photon energy (MeV)	Present Expt. $(\mu/\rho)(cm^2/gm)$	XCOM
0.0494	17.43 ± 1.34	18.30	0.0494	19.05 ± 1.46	19.09
0.0500	19.17 ± 1.42	17.74	0.0500	19.49 ± 1.47	18.50
0.0507	18.11 ± 1.23	17.12	0.0507	18.19 ± 1.56	17.84
0.0515	14.88 ± 1.50	16.44	0.0515	17.72 ± 1.66	17.13
0.0524	17.73 ± 1.40	15.72	0.0524	17.62 ± 1.39	16.38
0.0533	15.67 ± 1.09	15.05	0.0533	14.92 ± 1.19	15.67
0.0543	13.35 ± 0.95	14.34	0.0543	15.18 ± 1.03	14.94

Table 3.4: Comparison of measured values of attenuation coefficients, for Gd and Tb, with XCOM values.

Photon energy (MeV)	Present Expt. $(\mu/\rho)(cm^2/gm)$	XCOM	Photon energy (MeV)	Present Expt. $(\mu/\rho)(cm^2/gm)$	XCOM
0.0497	04.58 $\pm$ 0.33	03.92	0.0511	03.78 $\pm$ 0.37	03.84
0.0498	03.55 $\pm$ 0.25	03.90	0.0512	03.73 $\pm$ 0.27	03.82
0.0499	04.52 $\pm$ 0.31	03.88	0.0514	03.88 $\pm$ 0.30	03.78
0.0500	04.33 $\pm$ 0.28	03.86	0.0515	03.41 $\pm$ 0.32	03.77
0.0501	04.10 $\pm$ 0.24	03.84	0.0516	03.20 $\pm$ 0.33	03.75
0.0503	18.26 $\pm$ 1.34	18.58	0.0517	04.07 $\pm$ 0.35	03.73
0.0504	17.89 $\pm$ 1.22	18.48	0.0518	03.25 $\pm$ 0.34	03.71
0.0505	19.00 $\pm$ 1.28	18.39	0.0519	03.98 $\pm$ 0.35	03.69
0.0506	19.40 $\pm$ 1.36	18.29	0.0520	17.70 $\pm$ 1.61	17.76
0.0507	18.09 $\pm$ 1.31	18.20	0.0521	19.19 $\pm$ 1.58	17.67
0.0508	19.13 $\pm$ 1.17	18.11	0.0522	17.91 $\pm$ 1.58	17.58
0.0509	19.64 $\pm$ 1.33	18.01	0.0523	17.89 $\pm$ 1.50	17.50
0.0511	19.28 $\pm$ 1.37	17.83	0.0524	15.79 $\pm$ 1.74	17.41

References

[1] Th. Maternaa, J. Jolie, W. Mondelaersb and B. Masschaeleb, *Radiat. Phys. Chem* **59**, 449 (2000).

[2] M. Tamura, T. Akimoto, Y. Aoki, J. Ikeda, K. Satoa, F. Fujita, A. Homma, T. Sawamura and M. Narita, *Nucl. Instrum. Methods A* **484**, 642 (2002).

[3] G. Budak and R. Polat, *J. of Quant. Spectroscopy and Radiative Transfer* **88**, 525 (2004).

[4] U. Turgut, E. Buyukkasap, O. Simsek and M. Ertugrul, *Journal of Quantitative Spectroscopy and Radiative Transfer* **92**, 143 (2005).

[5] R. Polat, O. Icelli and G. Budak, *Analytica Chimica Acta* **505**, 307 (2004).

[6] N. Ramachandran, K. Karunakaran Nair, K. K. Abdullah and K. M. Varier, *Pramana* **67**, 507 (2006).

[7] B. P. Ajithkumar and E. T. Subramaniam, *Unpublished Report*, Nuclear Science Centre, New Delhi (1995).

[8] R. D. Evans, *The Atomic Nucleus*, (Tata McGrawHill), 714 (1955).

[9] M. J. Berger, J. H. Hubbel, S. M. Seltzer, J. S. Coursey and D. S. Zucker, *XCOM: Photon Cross Section Database (version 1.2)*. NIST, Gaithersburg, MD. (2003).

[10] M. J. Berger and J. H. Hubbell, *XCOM : Photon cross sections on a personal computer*, Program manual, NBS MD20899 (1990); M. J. Berger and J. H. Hubbell, XCOM version 3.1 - NIST Standard Reference Data Base (1999).

Chapter 4

Attenuation studies using PIXE on Zr, Nb, Mo and Pd around the K-edge

4.1 Introduction

The need for accurate experimental values for the X-ray attenuation coefficients (μ/ρ) has been increasingly demonstrated over the past few years consequent to the rapid advances made in the analytical methods using X-rays. The proton-induced X-ray-emission (PIXE) technique [1, 2] of trace-element analysis is one excellent example of these methods. Also, it has been shown that careful measurements of the attenuation coefficients give important information about the composition of materials like alloys, glasses, and biological tissues. The technique is widely used in different areas due to its possibilities in performing fast multi-elemental and nondestructive analysis of different kinds of samples. However, to convert the X-ray yields of different constituents of a thick sample to their concentrations, the X-ray mass attenuation coefficients are needed [3]. Since PIXE offers a low background yield, high sensitivity, mass attenuation coefficients derived using the technique offers excellent agreement between theory and experiment [4]. It is a unique technique for performing non-destructive analysis, which is based on the measurements of characteristic X-rays induced by the ener-

getic proton beam (MeV energy scale) directed onto the surface of a specimen [5]. This technique has been successfully used for almost three decades for analysis of various types of samples [6]-[14]. The reasons for use of PIXE as a method of choice for characterization of various materials are its well-known special features like multi-elemental capabilities, small sample mass requirements, high sensitivity, large dynamic range, and simple or virtually no sample preparation method.

In the present measurements, we have utilised the high energy proton beam to excite X-rays from a set of targets kept inside the pixe chamber. These X-rays are allowed to pass through the absorber placed inside the chamber, in front of the Si(Li) detector. The transmitted X-ray spectra are recorded and analyzed to find the attenuation coefficients. The experimental setup which consists of the Accelerator, PIXE chamber, detector, electronics and the measurement details are described in the next section.

4.2 Experimental setup

4.2.1 1.7 MV Tandetron Accelerator

The Particle Irradiation Faclity at the Indira Gandhi Centre for Atomic Research(IGCAR), Kalpakkam was used for the measurements using the PIXE method. Negative ion beam, extracted from an ion source(titanium hydride) is pre-accelerated to 30 keV, mass analysed by a 90^0 analysing magnet and injected into the accelerator. The ion beam gets accelerated to the positive high voltage terminal. At the high voltage terminal, the negative ions are stripped and the emerging positive ion beam is further accelerated. Depending on the positive charge state (q) attained during stripping, the energy of the beam for the terminal voltage of 1.7 MV will be Eq = 1.7(1+q). The positive ion beam is energy analysed by a switching magnet and switched to 10^0 or 30^0 ports in the left or in the right and the experimental set up can be installed in any of the ports. The whole operation of the machine and data collection is computer controlled.

4.2.2 PIXE Chamber

The scattering chamber used for experiments with the 2 MeV is made out of steel and has dimensions of 35 cm diameter and 38 cm height and is installed in one of the beam lines of the accelerator. Two graphite collimators of 4 mm dia each are put in the entrance to collimate the beam. It has various ports such

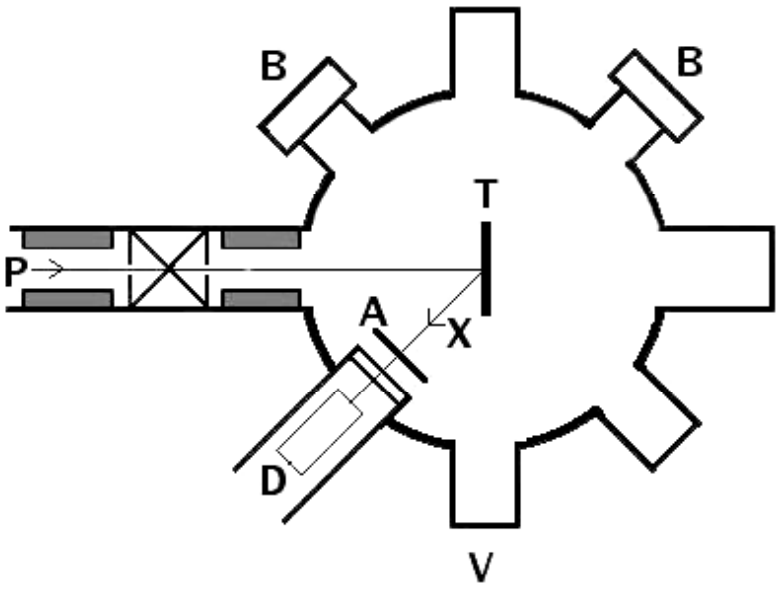

Figure 4.1: Schematic diagram of the experimental set up for gamma attenuation measurements using the PIXE method.

as feedthrough port, beam port, detector port and view port surrounding the chamber. The detector placed outside the vacuum is mounted on the detector port at an angle of 135^0. A mylar window of thickness 1.75 (mg/cm^2) has been fixed at the centre of the detector port. The target holder is an aluminum sheet of length 14 cm, width 3.5 cm and thickness 2 mm. The position of the targets mounted on the ladder can be changed from outside manually without breaking the vacuum. The chamber has several ports for viewing the beam on the target, for inserting detectors, for taking various cables into the chamber etc. The entire beam path from the ion source through the accelerating tubes and magnet chambers to the target chamber is maintained at a pressure of 10^{-8} to

10^{-7} Torr. A schematic drawing of the experimental arrangement is presented in Figure.4.1.

4.2.3 Source

A collimated beam of protons (P) were accelerated to 2 MeV in the Tandetron Accelerator at the centre. These energetic protons were allowed to bombard the target (T) mounted on a aluminium target ladder inside the cylindrical PIXE chamber. Turbo molecular pumps are installed at various locations for evacuating the entire proton beam path. The PIXE chamber, made out of stainless steel has a graphite beam collimator of 3 mm diameter to avoid the background X-rays originating from the scattered protons hitting the chamber walls. The vacuum inside the chamber is maintained through the port (V) and the ladder position can be adjusted by looking through the beam view port (B). In between the detector and the target there is a 100 micron mylar foil to filter the backscattered protons. Photographs of the experimental setup are given in Figures 4.1.1 and 4.1.2.

4.2.4 Electronics

The electronics and data acquisition system for the attenuation studies consists of a CANBERRA Si(Li) detector (D) with an active area of 30 mm^2 kept at an angle of 45^0 with the incident beam direction. The measuring system also includes a spectroscopy amplifier (ORTEC-672) and a Multi Channel Analyser (FAST COMTEC) with 8K ADC.

4.2.5 Targets and absorbers

The targets were 25 micron thin foils of Zr, Nb, Mo, Rh, Pd, Cd and Sn of size 1.5 cm x 1.5 cm, procured from Johnson Matthey Chemicals India Pvt. Ltd., Mumbai. The target holder was an aluminium ladder of size 15 cm x 3 cm. The position of the targets mounted on the ladder could be changed from outside

without breaking the vacuum. The X-ray beam (X) emerging from the target in the direction of the detector (D) can pass through the absorber (A). The absorbers are in the form of thin foils of size 1.5 cm x 1.5 cm and thickness 25 microns of elements Zr, Nb, Mo and Pd placed in front of the X-ray detector. The X-rays transmitted through the absorber were detected in a narrow beam geometry by the Si(Li) detector. Because of limitations on the geometry and dimensions of the PIXE chamber, the in-scattering angle in the narrow beam set up was around 5^0. The corresponding in-scattering correction was calculated to be less than 0.1% and the attenuation set up can be considered to be a narrow beam good geometry arrangement, which is an essential requirement for attenuation measurements. The proton current entering the scattering chamber was maintained at several nA. The X-ray exciter targets were irradiated for a preset total charge of typically 10 μC, as measured on the target ladder by using an ORTEC model 439 current digitizer.

4.2.6 Detector

A lithium drifted Si(Li) detector has been used to detect the X-rays produced by the protons. It is inserted at the chamber at an angle of 135^0 relative to the incident ion beam for X-ray direction. The 135^0 position has the advantage of a two fold reduction in electron bremsstrahlung background. The Si(Li)detector has the following characteristics:

Active area = 30 mm^2

Active diameter = 6.2 mm^2

Beryllium window thickness = $0.025mm$

Crystal thickness = $3mm$

Detector resolution = 160 eV at 5.9 keV

The distance of the detector from the centre of the chamber = 13.5 cm

4.2.7 Calibration of detector and electronics

Before the measurements of the attenuation coefficients can be attempted, the detector and the pulse processing electronics are to be calibrated. For this purpose one needs several standard gamma or X-ray lines of known energies. The radiations were obtained by irradiating elemental targets with the proton beam of energy 2 MeV. The characteristic X-rays from the elements provided the necessary calibration energies. The calibration curve has been plotted in Figure 4.2. It is seen that the calibration is quite linear in the energy region of interest.

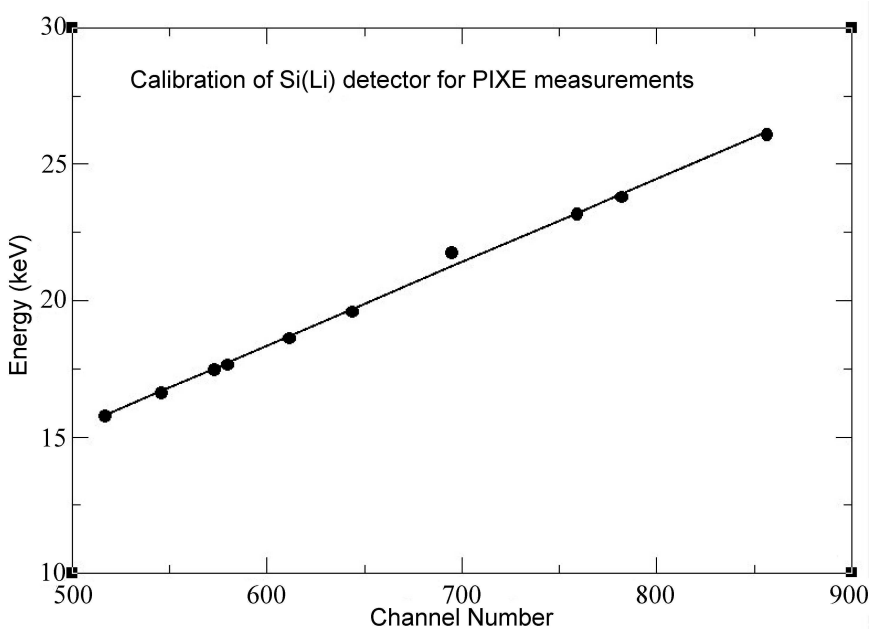

Figure 4.2: Calibration curve for the detector and electronics.

4.3 PIXE measurements

The present experiment is aimed at determination of the attenuation coefficients near the K-absorption edges for the metals Zn, Nb, Mo and Pd at energies around their K-absorption edges. The energies chosen were 15.74, 16.58, 17.44, 17.63, 18.70, 19.6, 20.16, 21.12, 22.71, 23.11, 23.81, 25.19, 26.17, 28.56 keV and were realized using secondary excitation from 25 micron thick foils of Zr, Nb, Mo, Rh, Pd, Cd and Sn. The main steps in the experimental procedure would

be to determine the intensities of the incident X-rays and those of the X-rays transmitted through the elemental absorbers. The number of incident X-rays depend on the protons incident on the exciter target, the target thickness and X-ray production cross section. Thus if we know the number of incident protons, the number of X-rays incident on the absorber is automatically known. The number of incident protons is measured by the charge collected on the target itself by means of the Current Integrator (CI).

A collimated beam of 2 MeV protons were allowed to fall on the exciter foil mounted on the target ladder at the centre of the pixe chamber. The beam current at the target was kept at 10 nA to reduce deadtime corrections and pile-up. The X-rays emitted by this foil at 45^0 to the incident proton beam were allowed to fall on the Si(Li) detector, with and without the absorber. The respective spectra were stored on the MCA connected to personal computer with the spectrum analysis software MCDWIN. It is a powerful - yet easy-to-use MCA Emulation software that operates under the MS-WINDOWS environment. It offers full software control of MCA-3 Series Multichannel Analyzers and TOF Time-of-Flight devices and extensive data manipulation capabilities and display functions. From the net counts under the characteristic peaks, the mass attenuation coefficients was calculated for the known absorber thickness, using Beer-Lambert Formula . Measurements were repeated for all possible combinations of exciter foil and absorber. Spectra were stored for the same preset charge (10 nC) collected on the ladder.

4.4 Results

Typical X-ray spectra for the direct beam and the beam transmitted through the absorbers have been shown in Figure 4.3. Counting times are roughly around 30 minutes for each spectrum. The attenuation coefficient values for the elements Zr, Nb, Mo and Pd obtained in the present measurements by the technique based on PIXE are presented in Tables 4.1 and 4.2. The errors associated with

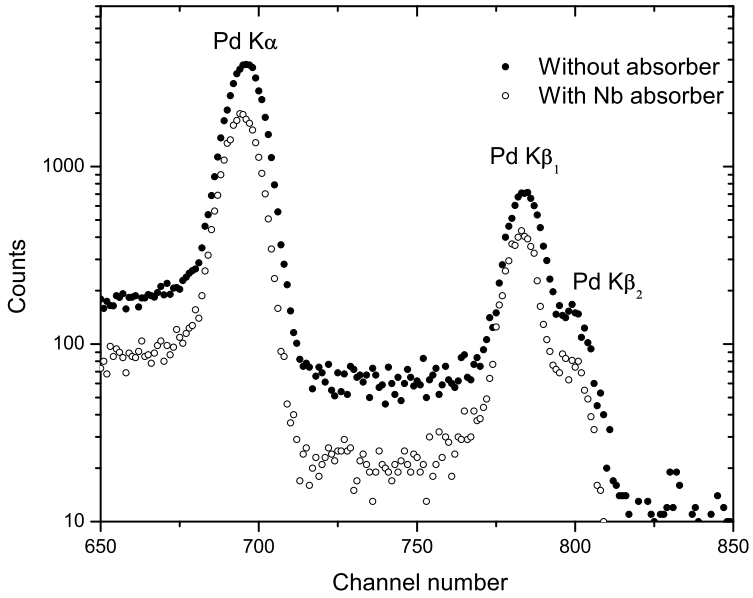

Figure 4.3: Spectra with and without a thin niobium foil absorber for proton excited Pd X-rays.

experimental (μ/ρ) data, due to statistical uncertainties in each case are also given. Also given for comparison, are the theoretical values obtained from the XCOM package. The plots obtained from these measurements are included in the next chapter for comparison with similar measurements using ^{241}Am radioactive source.

4.5 Discussion and Conclusions

The work described in this chapter aimed at determination of the attenuation coefficients near the K-absorption edges for the metals Zn, Nb, Mo and Pd at energies around their K-absorption edges. It can be seen from the results that the experimentally measured values of coefficients obtained in the present work agree reasonably well with the theoretical XCOM values. This gives confidence in the measurement techniques adopted. The data of Tamura *et al.* [15] for the range from 17.22 - 20.56 keV are also seen to be consistent with our data.

Table 4.1: Comparison of measured values of attenuation coefficients for Zr and Nb, with XCOM values.

Zr			Nb		
Photon energy (keV)	Present Expt. $(\mu/\rho)(cm^2/gm)$	XCOM	Photon energy (keV)	Present Expt. $(\mu/\rho)(cm^2/gm)$	XCOM
15.74	20.78±0.36	21.58	15.74	21.19 ± 0.43	23.41
16.58	16.58±0.28	18.74	16.58	17.96 ± 1.92	20.33
17.44	14.88±0.29	16.34	17.44	15.93 ± 0.32	17.72
17.63	18.33±1.47	15.87	17.63	15.83 ± 0.64	17.21
18.70	81.20±1.75	85.92	18.70	12.92 ± 0.39	14.68
19.60	69.71±2.02	76.23	19.60	76.40 ± 2.94	81.01
20.16	64.83±3.76	70.87	20.16	77.21 ± 4.48	75.52
21.12	59.80±1.33	62.90	21.12	64.93 ± 2.53	67.16
22.71	53.65±3.70	52.07	22.71	52.93 ± 3.65	55.72
23.11	46.82±1.42	49.78	23.11	50.47 ± 1.94	53.29
23.81	43.83±2.19	46.02	23.81	46.30 ± 2.69	49.29
25.19	38.69±0.86	39.64	25.19	40.81 ± 1.29	42.48
26.17	33.84±1.65	35.83	26.17	35.85 ± 2.45	38.41
28.56	26.23±1.54	28.30	28.56	28.07 ± 1.54	30.04

The present experiment, however covers a still wider range, 15.74 - 28.56 keV. . The energies chosen were $15.74 - 28.56$ keV and were realized using secondary excitation from 25 micron thick foils of Zr, Nb, Mo, Rh, Pd, Cd and Sn.

The attenuation measurements on Zr, Nb, Mo and Pd have also been done by using a radioactive source, ^{241}Am. The details of the experimental arrangement, procedure of taking measurements and its comparison with theory are included in the next chapter.

Table 4.2: Comparison of measured values of attenuation coefficients for Mo and Pd, with XCOM values.

Mo			Pd		
Photon energy (keV)	Present Expt. (μ/ρ)(cm^2/gm)	XCOM	Photon energy (keV)	Present Expt. (μ/ρ)(cm^2/gm)	XCOM
15.74	23.12 $\pm$ 0.44	24.97	15.74	30.80 $\pm$ 0.16	32.56
16.58	19.80 $\pm$ 1.85	21.66	16.58	25.97 $\pm$ 0.17	28.29
17.44	16.01 $\pm$ 2.45	18.86	17.44	22.43 $\pm$ 0.19	24.66
17.63	16.93 $\pm$ 0.49	18.30	17.63	22.24 $\pm$ 0.35	23.94
18.70	14.11 $\pm$ 0.54	15.61	18.70	19.86 $\pm$ 0.38	20.43
19.60	11.23 $\pm$ 0.34	13.79	19.60	16.98 $\pm$ 0.47	18.00
20.16	76.44 $\pm$ 3.68	79.49	20.16	12.50 $\pm$ 0.72	16.67
21.12	74.22 $\pm$ 2.24	77.11	21.12	14.50 $\pm$ 0.27	14.70
22.71	70.31 $\pm$ 4.15	68.10	22.71	09.28 $\pm$ 0.62	12.09
23.11	62.08 $\pm$ 2.00	65.39	23.11	12.19 $\pm$ 0.36	11.54
23.81	56.39 $\pm$ 2.88	60.43	23.81	10.52 $\pm$ 0.60	10.65
25.19	48.21 $\pm$ 1.39	50.90	25.19	54.15 $\pm$ 0.73	54.15
26.17	43.05 $\pm$ 2.47	44.83	26.17	49.46 $\pm$ 2.40	49.18
28.56	35.19 $\pm$ 1.78	33.08	28.56	35.00 $\pm$ 1.88	39.32

References

[1] S. A. E Johansson and J. L. Campbell, *PIXE, A Novel Technique for Elemental Analysis*, Wiley, Chichester UK, (1988).

[2] V. Havranek, V. Hnatowicz, J. Kvitek and I. Obrusnik, *Nucl. Instr. and Methods B* **85**, 637 (1994).

[3] J. L. Campbell and J. A. Cookson, *Nucl. Instr. and Methods B***3**, 185(1984).

[4] K. M. Varier and M. P. Unnikrishinan, *Phys.Rev.A*,**33** No.4,(1986)

[5] M. Kurosawa, S. Sueno and K. Shima *et al.*, *Nucl. Instrum. Methods B* **142**, 599 (1998).

[6] Z. Nejedly, J. Kral and J. Voltr *et al.*, *Nucl. Instrum. Methods B***136** 981 (1998).

[7] S. F. Bongiovanni, P. Prati, A. Zucchiatti, F. Lucarelli, P. A. Mando, V. Ariola and C. Bertone, *Nucl. Instrum. Methods B* **161**, 786 (2000).

[8] E. Jallot, J. L. Irigaray, G. Weber and P. Frayssinet, *In Surf. Interface Anal.* **27**, 648 (1999).

[9] R. Ashok Kumar, V. J. Kennedy, K. Sasikala, A. L. C. Jude, M. Ashok and Ph. Moretto, *Nucl. Instrum. Methods B* **190**, 449 (2002).

[10] P. A. Mando, *Nucl. Instrum. Methods B*, **85**, 815 (1994).

[11] P. Del Carmine, F. Lucarelli, P. A. Mando, and A. Pecchioli, *Nucl. Instrum. Methods B* **75**, 480 (1993).

[12] T. Calligaro, J. C. Dran, E. Ioannidou, B. Moignard, L. Pichon and J. Salomon, *Int. Conf. IBA, ECAART6* **14**, 21 (1999).

[13] A. Pwa, R. Siegele, D. D. Cohen, E. Stelcer and J. C. Van Moort, *Nucl. Instrum. Methods B* **190**, 501 (2002).

[14] R. J. Annegarn, C. S. Erasmus and J. P. F. Sellschop, *Nucl. Instrum. Methods B* **3**, 181 (1984).

[15] M. Tamura, T. Akimoto, Y. Aoki, J. Ikeda, K. Sato, F. Fujita, A. Homma, T. Sawamura and M. Narita, *Nucl. Instrum. Methods A* **484**, 642 (2002).

Chapter 5

X-ray attenuation studies using ^{241}Am gamma rays on Zr, Nb, Mo and Pd around the K-edge

5.1 Introduction

The present chapter describes the details regarding the measurements of the attenuation coefficients near the K-absorption edges for the metals Zn, Nb, Mo and Pd at energies around their K-absorption edges. As already mentioned in the previous chapter, we have resorted to a measurement method based on ^{241}Am gamma rays. The energies chosen were 15.74, 16.58, 17.44, 17.63, 18.70, 19.6, 20.16, 21.12, 22.71, 23.11, 23.81, 25.19, 26.17, 28.56 keV and were realized using secondary excitation [1]-[5] from 25 micron thick foils of Zr, Nb, Mo, Rh, Pd, Cd and Sn by using the radioactive source, ^{241}Am. The details of the experimental arrangement and procedure, the results derived therefrom, a comparison with the theory and conclusions drawn are described in the following sections.

5.2 Experimental method

The experimental set-up in the the present case consists of the radioactive source, target and absorbers, detector and electronics, as shown in Figure 5.1. These

components are described in the following section.

5.2.1 Source

The 300 mCi, ^{241}Am source for the present measurements had been procured from M/s Amersham, England. This source provided 59.54 keV gamma rays which were used as exciters in place of the proton beams in the set up using the PIXE method. Characteristic X-rays required for the present measurements are emitted when the gamma rays are directed towards the target. The source (S) was well shielded and a narrow gamma ray beam obtained by means of a collimator (C).

5.2.2 Targets and absorbers

A secondary X-ray exciter target (T) was kept in front of the ^{241}Am source. The targets (25 micron thin foils of Zr, Nb, Mo, Rh, Pd, Cd and Sn of size 1.5 cm x 1.5 cm) and absorbers (25 micron thin foils of Zr, Nb, Mo and Pd of size 1.5 cm x 1.5 cm) for the measurements were the same as used in the PIXE studies. The X-rays generated from the targets in forward direction were again collimated and allowed to fall on the absorber (A) which ensured a narrow beam good geometry [6] set up for attenuation measurements. Figure 5.1.1 shows a photograph of the

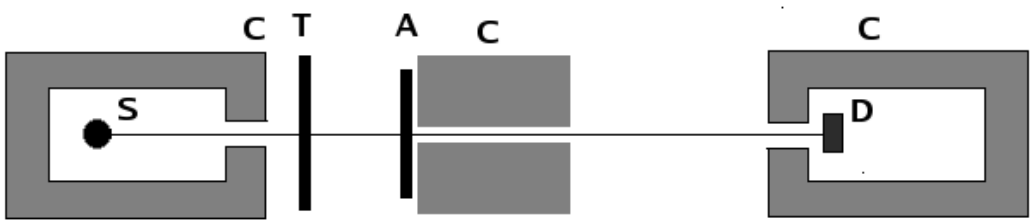

Figure 5.1: Schematic diagram of the experimental set up for narrow beam geometry gamma attenuation measurements using ^{241}Am source.

experimental arrangement.

5.2.3 Detector and Electronics

The detector for the transmitted X-rays was an ORTEC HPGe Gamma X detector with a resolution of 1.14 keV at 59.54 keV. The output pulses were shaped and amplified by an ORTEC 571 amplifier. The amplified output pulses were then fed to a CAMAC based data acquisition and analysis system, consisting of a Kinetic CAMAC crate, crate controller, a 4k Quad ADC, supplied by the Electronics Division, BARC and connected to a Personal Computer through a suitable interface card. The Linux based FREEDOM software [7], developed at the Inter University Accelerator Center, New Delhi is used in the present investigations for both online data acquisition and for online as well as offline data analysis. Details of the software have been described earlier in chapter 3.

5.2.4 Experimental procedure

Calibration of the detector and electronics was done as described in chapter 3. The exciter foil was positioned in front of the ^{241}Am source. The characteristic X-rays emitted from the exciter foil were detected first directly without any absorber in the path of the X-rays. The absorber was then introduced in the path and the spectrum of the transmitted X-rays was stored for the same time interval. The attenuation coefficient value was extracted from the ratio of the peak areas with and without the absorber.

5.2.5 Data Analysis

Spectra of the X-rays were taken with and without each absorber in their paths. The peak areas for the direct X-rays and the X-rays transmitted through absorber were extracted from the spectra. The mass attenuation coefficients are then calculated from the relation

$$I = I_0 exp[-(\mu/\rho)x\rho] \tag{5.1}$$

where μ is the linear attenuation coefficient(cm^{-1}), ρ is the density of the sample (gcm^{-3}), x is the thickness of the absorber (cm), I_0 is the count value without

the sample and I is the count value of the radiation penetrating through the sample. In-scattering contributions in both the PIXE method and the ^{241}Am source method were found to be much small compared to the experimental uncertainties.

5.3 Results

Typical X-ray spectra for the direct beam and the beam transmitted through the absorbers have been taken for roughly around 30 minutes for each spectrum. The mass attenuation coefficients, determined in the present work using the technique secondary excitation by ^{241}Am gamma rays, are presented in Tables 5.1 and 5.2. For comparison, theoretical values obtain from the XCOM package are also provided.

Table 5.1: Comparison of measured values of attenuation coefficients for Zr and Nb, with XCOM values.

Zr			Nb		
Photon energy (keV)	Present Expt. $(\mu/\rho)(cm^2/gm)$	XCOM	Photon energy (keV)	Present Expt. $(\mu/\rho)(cm^2/gm)$	XCOM
15.74	19.03 $\pm$ 0.55	21.58	15.74	26.80 $\pm$ 0.91	23.41
16.58	20.48 $\pm$ 0.44	18.74	16.58	17.92 $\pm$ 0.73	20.33
17.44	17.47 $\pm$ 0.53	16.34	17.44	14.27 $\pm$ 0.41	17.72
17.63	12.42 $\pm$ 1.30	15.87	17.63	18.51 $\pm$ 0.82	17.21
18.70	83.68 $\pm$ 3.86	85.92	18.70	11.87 $\pm$ 0.77	14.68
19.60	71.94 $\pm$ 2.99	76.23	19.60	74.38 $\pm$ 3.40	81.01
20.16	67.40 $\pm$ 3.45	70.87	20.16	80.01 $\pm$ 4.30	75.52
21.12	66.40 $\pm$ 2.67	62.90	21.12	68.23 $\pm$ 2.86	67.16
22.71	50.33 $\pm$ 3.51	52.07	22.71	48.45 $\pm$ 3.20	55.72
23.11	47.93 $\pm$ 1.87	49.78	23.11	53.78 $\pm$ 2.61	53.29
23.81	39.88 $\pm$ 2.40	46.02	23.81	45.07 $\pm$ 2.69	49.29
25.19	36.20 $\pm$ 1.40	39.64	25.19	41.98 $\pm$ 2.11	42.48
26.17	37.43 $\pm$ 1.90	35.83	26.17	39.09 $\pm$ 2.28	38.41
28.56	25.40 $\pm$ 1.61	28.30	28.56	33.41 $\pm$ 2.30	30.40

The attenuation coefficient values, obtained in the present measurements by the two different techniques based on PIXE (previous chapter) and ^{241}Am source are plotted as a function of the X-ray energy in Figures 5.2-5.5. The

Table 5.2: Comparison of measured values of attenuation coefficients for Mo and Pd, with XCOM values.

Mo			Pd		
Photon energy (keV)	Present Expt. $(\mu/\rho)(cm^2/gm)$	XCOM	Photon energy (keV)	Present Expt. $(\mu/\rho)(cm^2/gm)$	XCOM
15.74	21.29 $\pm$ 0.62	24.97	15.74	34.41 $\pm$1.07	32.56
16.58	18.90 $\pm$ 0.59	21.66	16.58	27.26 $\pm$0.57	28.29
17.44	21.41 $\pm$ 0.39	18.86	17.44	21.04 $\pm$0.47	24.66
17.63	15.25 $\pm$ 0.59	18.30	17.63	18.83 $\pm$0.77	23.94
18.70	13.08 $\pm$ 0.68	15.61	18.70	24.24 $\pm$1.35	20.43
19.60	16.20 $\pm$ 0.63	13.79	19.60	17.43 $\pm$0.68	18.00
20.16	74.38 $\pm$ 4.14	79.49	20.16	14.40 $\pm$0.68	16.67
21.12	80.23 $\pm$ 2.29	77.11	21.12	12.59 $\pm$0.41	14.70
22.71	63.71 $\pm$ 4.41	68.10	22.71	09.24 $\pm$0.59	12.09
23.11	60.02 $\pm$ 1.89	65.39	23.11	13.28 $\pm$0.44	11.54
23.81	54.34 $\pm$ 2.13	60.43	23.81	08.98 $\pm$0.48	10.65
25.19	47.84 $\pm$ 1.67	50.90	25.19	49.96 $\pm$1.34	54.15
26.17	51.30 $\pm$ 2.34	44.83	26.17	52.00 $\pm$2.89	49.18
28.56	28.03 $\pm$ 1.41	33.08	28.56	35.59 $\pm$1.78	39.32

errors associated with experimental (μ/ρ) data, due to statistical uncertainties in each case are also shown. The respective K-edge energies are also given in these figures. The XCOM values are plotted in the form of solid curves for comparison. In addition, we have plotted the experimental results of Tamura *et al.* [8] for the elements Zr, Nb and Mo.

5.4 Discussion and Conclusions

It can be seen from Figures 5.2 -5.5 that the two sets of experimental results for the attenuation coefficients obtained in the present work agree reasonably well with each other and also with the XCOM values. This gives confidence in the measurement tehniques adopted in both sets of measurements. The data of Tamura *et al.* [8] for the range from 17.22 - 20.56 keV are also seen to be consistent with our data. The present experiment covers a still wider range, 15.74 - 28.56 keV. The better accuracy of the PIXE results is worth mentioning in this context. This is obviously due to the larger intensities of the incident X-

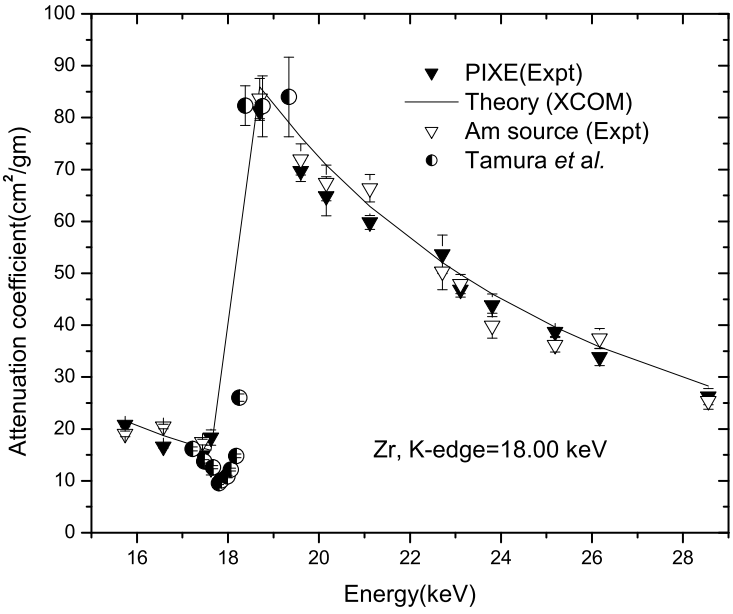

Figure 5.2: Comparison of the present experimental results obtained by the PIXE and ^{241}Am methods with XCOM values for Zr.

rays available with this technique as well as the relatively lower background levels. We feel therefore that further investigations on X-ray attenuation near K-edge energies using the PIXE technique would be highly desirable for other elements also. Keeping in view the fairly close comparison of the present results with theory, calculation of dispersion corrections to the forward Rayleigh scattering amplitude [9, 10] of the elements Zr, Nb, Mo and Pd had also been attempted therefrom. Details of the calculations and the results are given in the next chapter.

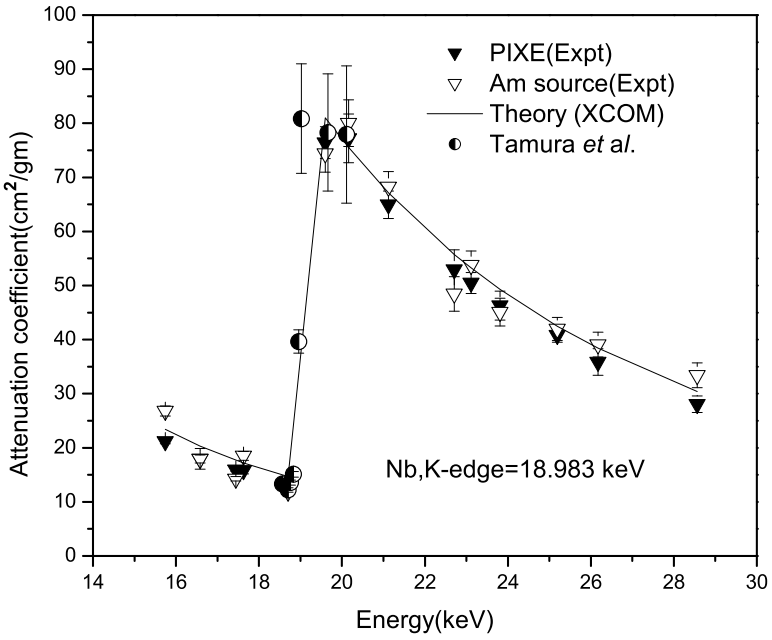

Figure 5.3: Comparison of the present experimental results obtained by the PIXE and ^{241}Am methods with XCOM values for Nb.

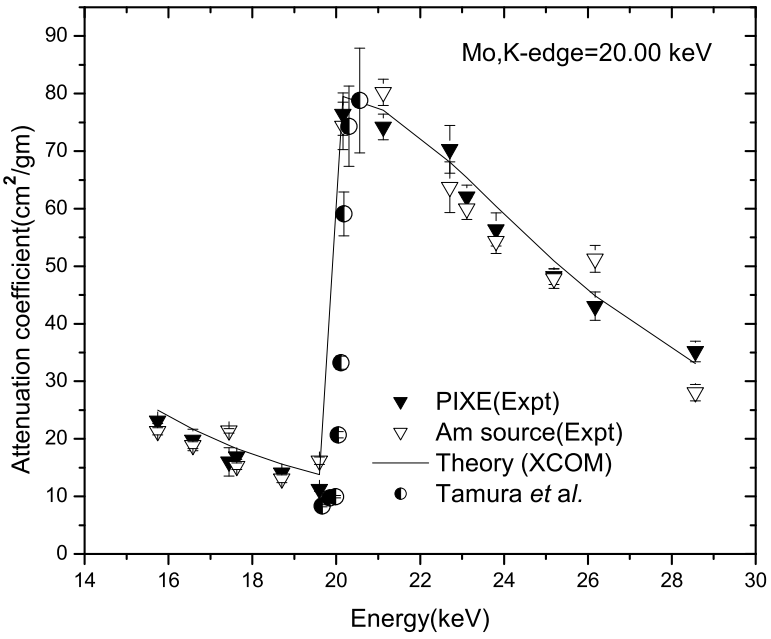

Figure 5.4: Comparison of the present experimental results obtained by the PIXE and ^{241}Am methods with XCOM values for Mo.

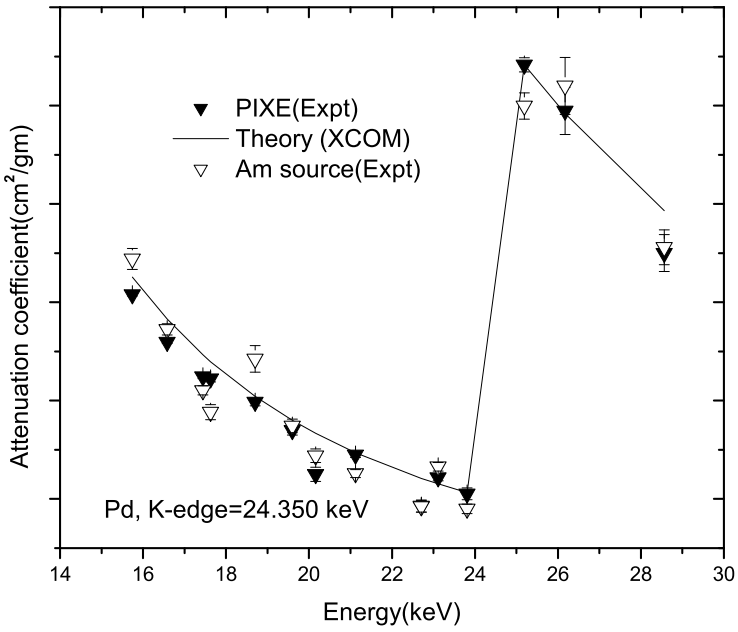

Figure 5.5: Comparison of the present experimental results obtained by the PIXE and ^{241}Am methods with XCOM values for Pd.

References

[1] S. M. Midgley, *Radiation Physics and Chemistry* **72**, 525 (2005).

[2] U. Turgut, E. Buyukkasap, O. Simsek and M. Ertugrul, *J. of Quant. Spectr. and Radiat.Transfer* **92**, 143 (2005).

[3] A. Karabulut, A. Gurol, G. Budak and M. Ertugrul, *Nucl.instr. and Methods in Phys. Research B* **227**, 485 (2005).

[4] Ug ur Cevika, Hasan baltasb, A. Celika and E. Bacaksiza, *Nucl. Instrum. Methods B* **247**, 173 (2006).

[5] U. Turgut, O. Simsek, E. Buyukkasap and M. Ertugrul, *Spectrochim.Acta Part B* **57**, 261(2002).

[6] P. P. Kane, G. Basavaraju and K. M. Varier, *Nucl. Instr. and Methods in Phys. Research Section B* **149**, 379 (1999).

[7] B. P. Ajithkumar and E. T. Subramaniam, *Unpublished Report*, Inter University Accelerator Centre, New Delhi. (1995).

[8] M. Tamura, T. Akimoto, Y. Aoki, J. Ikeda, K. Sato, F. Fujita, A. Homma, T. Sawamura and M. Narita, *Nucl. Instrum. Methods A* **484**, 642 (2002).

[9] S. B. Appaji Gowda and T. K. Umesh, *Nucl. Instrum. Methods B* **243**, 2 (2006).

[10] M. Kefi, J. M. Andre, Y. Heno, G. Giorgi and C. Bonnelle, *Phys. Rev. A* **45**, 2859 (1992).

Chapter 6

Anomalous Scattering factors

6.1 Introduction

Electrons occupy definite energy levels within the atom and are characterized by natural angular frequency. When a photon interacts with electron of the atom, the natural amplitude of the electron is modified by, a dispersive term dependent on the proximity of the impressed frequency to the natural resonant frequency of the system and an absorptive term, dependent on the damping factor for the resonant system. This results in the anomalous scattering of photons.

The basic description of anomalous scattering in terms of scattering cross section of an atom as seen by an incident X-ray photon can be explained as follows. When the incident photon has relatively low energy, the photon is not absorbed as it has insufficient energy to excite any of the available electronic transitions. The scattering cross-section of the atom (the probability that the photon is scattered) can be adequately described in using normal atomic scattering coefficient f_0, also called atomic form factor. The photon scatters without phase delay and imaginary component of scattering coefficient f'' is zero. When the incident photon has high enough energy, some photons are scattered normally, some photons are absorbed and re-emitted at lower energy (fluorescence) and some photons absorbed and re-emitted immediately at the same energy (strong coupling to the absorption edge energy). Then the scattered photon gains an imaginary component $f"$ to its phase and is retarded compared to normally scattered photon.

This effect is measured as a function of X-ray energy by noting either the sharp increase in absorption or in fluorescence. The Figure 6.1, as given from the calculations of Cromer and Liberman [1] illustrates anomalous scattering effect. Thus,

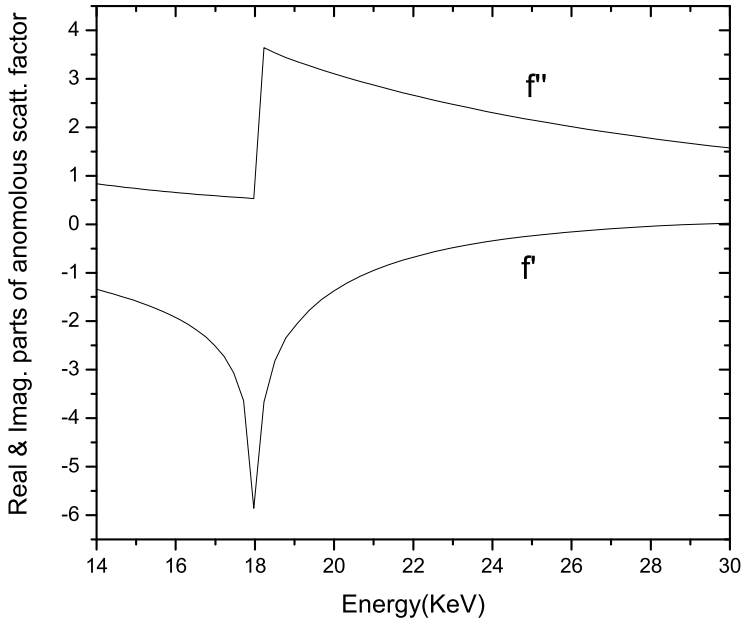

Figure 6.1: Theoretical variation of the real and imaginary scattering components, f' and f'' for the element Zr . The f' values are derived from the corresponding f'' spectra via the Kramers-Kronig equation.

the anomalous X-ray scattering from an atom is described by a modification of the scattering factor. It becomes a complex quantity and is written as

$$f = f_0 + f^{'} + if^{"}, \tag{6.1}$$

where first term f_0 is the Thomson scattering form factor, $f^{'}$ and $f^{"}$ are real and imaginary parts of anomalous scattering factors also known as dispersion corrections.

6.2 Description of anomalous scattering factor

The concept of atomic scattering factor has its origin in the classical electromagnetic theory [2]-[5]. Consider the scattering of an unpolarized electromagnetic

wave by a free electron, a process known as Thomson scattering. For a free electron situated at the origin the fraction of intensity of the scattered wave through an angle ϕ is [6]

$$\frac{I}{I_0} = (\frac{r_0}{r})^2 \frac{1}{2}(1 + cos^2\phi), \tag{6.2}$$

where r_0 is the classical electron radius and r is the distance measured along the scattering direction at which the intensity is measured. Considering the scattering of electromagnetic waves by the electrons bound to an atom, each electron scatters as an individual electron and the atomic scattering is the sum of each of these individual contributions. Since the electrons are not localized in space, but are in rapid motion about the nucleus the atomic scattering factor can be written in terms of the electron density ρ, which exists at a distance r from the nucleus. Also, because the size of the atom is comparable with the wavelength of incident electromagnetic wave, an electron within the atom will scatter as though its scattering factor is

$$f = \int \exp(\frac{2\pi i}{\lambda})(\overrightarrow{k_f} - \overrightarrow{k_i})\rho dV \tag{6.3}$$

where $\overrightarrow{k_f}$-$\overrightarrow{k_i}$ is the change in the direction of the wave vector of the electromagnetic wave. The scattering factor f is thus the Fourier transform of the electronic charge distribution ρ and is alternatively referred to as the atomic scattering factor. If the atom is assumed to have a charge distribution with spherical symmetry, eq. (6.3) can be simplified as

$$f = 4\pi \int_0^\infty \rho(r) r^2 \frac{sin(qr)}{qr} dr, \tag{6.4}$$

where $\rho = \rho(r)$, $q = |\overrightarrow{k_f} - \overrightarrow{k_i}| = (4\pi sin\theta/\lambda)$, and $\theta = \phi/2$. The assumption of spherical symmetry for electron charge distribution is reasonable since the orbital involved directly in the scattering processes are often called shells and therefore have spherical symmetry. For an atom containing several electrons the atomic scattering factor becomes

$$f = \Sigma_n 4\pi \int_0^\infty \rho_n(r) r^2 \frac{sin(qr)}{qr} dr, \tag{6.5}$$

For forward scattering ($\theta = 0$) the value of $sin(qr)/qr$ becomes unity and the scattering factor f equal to Z, the total number of electrons in the atom. Thus

$$Z = \Sigma_n 4\pi \int_0^\infty r^2 \rho_n(r) dr. \tag{6.6}$$

In general, the radial distribution of electron density $\rho(r)$ must be known before f can be determined. The effect of anomalous scattering can most simply be described by treating an electron as a classical dipole oscillator driven by a force affected by the incident X-ray and with damping corresponding to the bound state in which the electron exists. Consider a bound electron placed at the origin having a damping constant γ and a natural resonant frequency ω_0. An X-ray of frequency ω is incident on the electron with an electric field vector at time t at the electron given by $\overrightarrow{E} = \overrightarrow{E_0} \exp(i\omega t)$. The electron is forced into motion by the presence of the oscillating electric field and at time t, has a displacement x, perpendicular to the direction of travel of the X-rays, described by the equation of motion,

$$\ddot{x} + \gamma \dot{x} + \omega_0^2 x = \frac{eE_0}{m} \exp(i\omega t) \tag{6.7}$$

The solution to this equation will have the form

$$x = \frac{eE_0 \exp(i\omega t)}{m(\omega_0^2 - \omega^2 + i\gamma\omega)} \tag{6.8}$$

The axis of the dipole is parallel to the direction of the incident electric vector $\overrightarrow{E}$. The oscillating dipole is the source of an electromagnetic wave of same frequency. The amplitude of the scattered wave at unit distance from the equatorial plane of the dipole is

$$E_{max} = \frac{e^2\omega^2 E_0}{c^2 m(\omega_0^2 - \omega^2 + i\gamma\omega)} \tag{6.9}$$

The analogous expression for a free electron acting as a dipole oscillator may be obtained by letting $\omega_0 = \gamma = 0$.

$$E'_{max} = \frac{e^2\omega^2 E_0}{c^2 m(-\omega^2)} \tag{6.10}$$

Now we obtain a result for the scattering factor of a single bound electron with resonant frequency ω_0, and damping constant γ for incident X-rays of frequency

ω, as the ratio of amplitude scattered by the oscillator to the amplitude scattered by a free classical electron under same condition. i.e.,

$$f = \frac{E_{max}}{E'_{max}} = \frac{\omega^2}{(\omega^2 - \omega_0^2 - i\gamma\omega)} \tag{6.11}$$

It can be seen that the scattering factor is a complex quantity due to the effects of the damping term. If $\omega >> \omega_0$, f is positive and the scattered wave is opposite in phase with the incident wave. If $\omega << \omega_0$, f is negative and the dipole then scatters the wave in phase with the primary wave. When $\omega \approx \omega_0$, the scattering factor become complex, which means that both the amplitude and phase of the scattered radiation depend on the incident frequency. We may split this expression into real and imaginary parts by multiplying top and bottom with $(\omega_0^2 - \omega^2 + i\gamma\omega)$ and separating out the terms. Then we obtain,

$$f = (\frac{\omega^2(\omega^2 - \omega_0^2)}{(\omega^2 - \omega_0^2)^2 + \gamma^2\omega^2}) + i(\frac{\gamma\omega^3}{(\omega^2 - \omega_0^2)^2 + \gamma^2\omega^2}) \tag{6.12}$$

which is equivalent to the expression

$$f = f_1 + if_2, \tag{6.13}$$

where f_1 and f_2 are the dispersive and absorptive terms respectively. The first term on the right hand side includes the Thompson scattering term and the real part of the anomalous scattering correction. Again we notice that as $\gamma \to 0$ and $\omega_0 \to 0$ $f \to 1$. In order to show classically that the first term of eq.(6.12) does indeed correspond to $f_0 + f'$ it is necessary to assume that the damping constant is small.

We now let the atom contain N oscillators, each represented by an oscillator strength g_j and each having natural frequency ω_j . The oscillator strengths g_j quantify the contribution of each electron to the scattering factor and are assumed to comply to the Thomas-Reiche-Kuhn [7, 8, 9] sum rule,

$$\sum_{j=1}^{N} g_j = Z. \tag{6.14}$$

In the quantum mechanical treatment of anomalous scattering the values are proportional to the transition probabilities between initial and final energy states.

With the assumption that only the inner core electron states K, L, .. contribute to anomalous scattering, we may rewrite the real part of eq.(6.12) as

$$f_1 = f_0 + f' = \sum_{j=1}^{N} g_j - \sum_{K,L..} \frac{g_j \omega_j}{\omega_j^2 - \omega^2}, \tag{6.15}$$

where f_0, called the form factor, represents the sum of all the elements of the set of oscillator strengths and is unity for a single electron atom. i.e.,

$$f_0 + f' = Z - \sum_{K,L..} \frac{g_j \omega_j}{\omega_j^2 - \omega^2}, \tag{6.16}$$

where Z equals the Thompson scattering component for forward scattering. In an atom, effectively infinite number of oscillator states exists and hence the second term of the above equation can be written as

$$f' = \int_{\omega}^{\infty} \frac{\omega^2 (dg/d\omega)}{\omega_0^2 - \omega^2} d\omega, \tag{6.17}$$

where the atom is assumed to have infinite number of energy states. For an atom containing k electrons f' is given by

$$f' = \Sigma_k \int_{\omega}^{\infty} \frac{\omega^2 (dg/d\omega)_K}{\omega_0^2 - \omega^2} d\omega. \tag{6.18}$$

The oscillator strength of k^{th} electron is given by

$$g_k = \int_{\omega}^{\infty} (\frac{dg}{d\omega}) d\omega. \tag{6.19}$$

The imaginary part to the scattering factor f'' is associated with the damping of the incident wave by the bound electrons. It is therefore related to linear coefficient of absorption μ of the material which can be determined from experimental measurement of the decrease in intensity of the photon beam as it passes through a medium containing atoms under investigation. The attenuation coefficient per atom μ_a is related to the density of the oscillator states by

$$\mu_a = \frac{\pi^2}{2\epsilon_0 mc} (dg/d\omega) \tag{6.20}$$

The imaginary part of the anomalous scattering correction f'', is

$$f'' = \frac{\pi\omega}{2} (dg/d\omega). \tag{6.21}$$

i.e, $f^{'}$is related to $f^{''}$ through the relation,

$$f^{'} = \frac{2}{\pi} \sum_{k} P \int_{\omega}^{\infty} \frac{\omega f^{''}(\omega)}{\omega_0^2 - \omega^2} d\omega. \tag{6.22}$$

This is referred to as the Kramers-Kronig transform. Eqs. (6.18), (6.21) and (6.22) are the fundamental equations of the classical theory of photon scattering. Then the linear absorption coefficient per atom $\mu_a \equiv \sigma_{tot}$, which is the total cross section, and $f^{"}$ can be written as

$$f^{''} = \frac{mc\epsilon_0\omega}{\pi} \sigma_{tot}. \tag{6.23}$$

This is one form of the Optical theorem [10]. This relationship is important as it allows direct experimental measurement of $f^{"}$ for a scatterer via measurement of its atomic absorption cross-section. In terms of the incident X-ray energy, $E = \hbar\omega$, the Optical theorem may be written

$$f^{''} = \frac{mc\epsilon_0 E}{e^2\hbar} \sigma_{tot}. \tag{6.24}$$

In terms of classical electron radius r_0, we obtain the expression as

$$f^{''} = \frac{E}{2hcr_0} \sigma_{tot}. \tag{6.25}$$

Here, ($r_0 = \frac{e^2}{4\pi\epsilon_0 mc^2}$)is the classical electron radius also known as the Compton radius or the Thomson scattering length is based on a classical relativistic model of the electron. Its value is calculated as $2.817940325 \times 10^{-15} m$. The total cross section σ_{tot} is given by $\sigma_{tot} = \tau + \sigma_{BBT} - \sigma_{BPP}$, where τ, σ_{BBT}, σ_{BPP} are the photoeffect, photoexcitation, and bound pair production cross-sections respectively. For energies sufficiently away from absorption edges of a particular element, σ_{BBT}, σ_{BPP} are expected to be insignificant for $Z > 10$, below the pair production threshold [11, 12].

In the region of current interest, if we neglect the spin flip process, the $f^{'}$ and $f^{"}$ are connected by modified Kramers-Kronig transform [13, 14] given by

$$f_R^{'}(E) = f^{'}(\infty) - \frac{2}{\pi} P \int_0^{\infty} \frac{E^{'} f^{"}(E^{'})}{E^2 - E^{'2}} dE^{'}, \tag{6.26}$$

where P is the Cauchy principal value of the dispersion integral. The second term on the R.H.S.of the above equation represents the non-relativistic values

$f'_{NR}(E)$. These values are found to be at variance with the theoretical values by a factor $f'(\infty)$ which is called high-energy limit or relativistic correction. It is negative and generally independent of energy. The $f'(\infty)$ values of Cromer and Liberman (CL) [1], Creagh and McAuley (CM) [6] and Kissel and Pratt (KP) [15] for elements Zr, Nb, Mo and Pd are given in Table 6.1.

Table 6.1: Relativistic corrections (high energy limit, $f'(\infty) = \triangle$)

Element	$\triangle_{KP}$ S-matrix correction	$\triangle_{CM}$ Multiple correction	$\triangle_{CL}$ Dipole corrections
Zirconium	-0.181	-0.192	-0.319
Niobium	-0.191	-0.204	-0.338
Molybdenum	-0.203	-0.216	-0.359
Palladium	-0.251	-0.270	-0.447

6.3 Calculation of real part of the anomalous scattering factor

The dispersion correction $f'(E)$ was determined by the numerical evaluation of the dispersion integral in eq.(6.4). For this purpose, the lower limit of integration was chosen to be 1 keV, the M_V absorption edge and upper limit was 1500 keV. To evaluate the integral numerically,the energy region used for integration was divided into a large number of small intervals. Within each interval (E_i, E_{i+1}), The energy dependence of $f_i^{"}$ was determined by a linear function.

$$f_i^{"} = a_i + b_i E \tag{6.27}$$

In this interval, the dispersion integral assumes the form

$$I_{i,i+1}(E_s) = \frac{2}{\pi} P \int_{E_i}^{E_{i+1}} \frac{E' f^{"}(E')}{E_s^2 - E'^2} dE'. \tag{6.28}$$

Mathematically the above equation is equivalent to

$$I_{i,i+1}(E_s) = \frac{2}{\pi}[\frac{a_i}{2} \ln|\frac{E_s^2 - E_{i+1}^2}{E_s^2 - E_i^2}|$$
$$+b_i((E_{i+1} - E_i - \frac{E_s}{2} \ln|\frac{(E_{i+1} + E_s)(E_i - E_s)}{(E_{i+1} - E_s)(E_i + E_s)}|)]. \tag{6.29}$$

Using the coefficients a_i and b_i the dispersion integral in equation 6.28 was calculated as explained in the following section.

6.4 Evaluation of the Dispersion Integral

As explained in chapter 4, the present experimental measurements of the attenuation coefficients for the elements Zr, Nb, Mo and Pd cover the energy range of 15.74 to 28.56 keV, we have adopted the following values of the photoelectric cross sections for the evaluation of the integral ,

1. Below the lower energy limit (Emin = 15.74 keV) of the present measurements, down to 1 keV, XCOM values

2. In the range $15.74 \leq E_r \leq 28.56$, (Emax= 28.56 keV, the upper energy limit of the present work), the photoelectric cross sections extracted from the measured attenuation coefficients, after subtracting the relatively small coherent and incoherent scattering contributions.

3. Above the upper limit (28.56 keV) to 1500 keV, XCOM values [16, 17]. We have arbitrarily fixed the limits of integration in the dispersion integral as E1 = 1 keV and E2 = 1500 keV. The evaluations have been repeated by varying these limits and it was verified that the change in the calculated corrections are negligible when these limits are changed by 10%.

The required integrals in eq. (6.4) have been evaluated using a semi-analytical, semi-numerical approach. At each energy Ei, the integral to be evaluated is

$$I(E_i) = \int_{E_1}^{E_2} \frac{E\sigma_{ph}(E)dE}{E_i^2 - E^2} = \int_{E_1}^{E_0} \phi(E)dE, \tag{6.30}$$

where, $\phi(E) = E\sigma_{ph}(E)/(E_i^2 - E^2)$. The integral is then split into three components:

a) from E_1 to $E_i - \epsilon$

b) from $E_{i-\epsilon}$ to $E_i + \epsilon$

c) from $E_{i+\epsilon}$ to E_2

Thus

$$I(E_i) = \int_{E_1}^{E_{i-\epsilon}} \phi(E)dE + \int_{E_{i-\epsilon}}^{E_{i+\epsilon}} \phi(E)dE + \int_{E_{i+\epsilon}}^{E_2} \phi(E)dE. \tag{6.31}$$

i.e.,

$$I(E_i) = I_1(E_i) + I_2(E_i) + I_3(E_i). \tag{6.32}$$

Here ϵ is an arbitrarily chosen small energy interval (typically taken as $Ei/1000$). For evaluating $I_1(E_i)$ and $I_3(E_i)$, the relevant energy interval is subdivided further into a large number of equal sub intervals (on a logarithmic scale). Within each sub interval the integration is carried out using Simpson's rule, assuming a linear variation of the photoelectric cross section.

$$\ln(\sigma_{ph}(E)) = a + b\ln(E). \tag{6.33}$$

In the energy region below the lower energy limit and above upper energy limit of the present measurements, the XCOM values of the photoelectric cross sections are directly used for the integration. For evaluating I_2, eq. (6.29) has been used. Based on the above procedure, the dispersion integral and consequently the real part of the anomalous scattering factor was evaluated numerically using a fortran program, a flow chart of which is included in APPENDIX-II.

6.5 Results and conclusions

From the experimental values of attenuation coefficients (Tables 5.1 and 5.2) obtained from the measurements described in the previous chapter, the photoeffect cross sections (σ_{ph}) were derived by subtracting the sum of the corresponding coherent and incoherent scattering cross sections for the elements Zr, Nb, Mo and Pd at all the energies of present interest. These values of (σ_{ph}) yielded the imaginary part of the anomalous scattering factor as per eq. (6.25). Knowing the values of f'' and taking account of the relativistic corrections (KP, CM and CL) tabulated in Table 6.1, the f' values were obtained by evaluating the dispersion integral as per the procedure mentioned above. The photoeffect cross sections,

the real and imaginary parts of the anomalous scattering factors in the case of Zr, Nb, Mo and Pd around K-edge are tabulated in Tables 6.2 to 6.4.

Table 6.2: Photo effect cross-sections(σ_{tot}), imaginary part (f'') and real part (f') of the anomalous scattering factor for *Zr*

Energy	σ_{tot}	f''	Real Part, f'		
(keV)	($barns/atom$)		(KP)	(CM)	(CL)
15.74	02941.65	0.66	-1.55	-1.54	-1.68
16.58	02317.90	0.55	-1.97	-1.96	-2.10
17.44	02071.91	0.52	-2.88	-2.87	-3.01
17.63	02596.78	0.66	-3.28	-3.27	-3.40
18.70	12131.27	3.25	-2.16	-2.15	-2.28
19.60	10400.13	2.92	-1.40	-1.39	-1.53
20.16	09666.34	2.79	-1.19	-1.19	-1.31
21.12	08912.64	2.69	-0.91	-0.89	-1.03
22.71	07993.17	2.60	-0.35	-0.34	-0.48
23.11	06961.41	2.30	-0.26	-0.25	-0.39
23.81	06512.66	2.22	-0.26	-0.25	-0.39
25.19	05742.66	2.07	-0.11	-0.10	-0.23
26.17	05013.20	-0.03	-0.01	-0.01	-0.15
28.56	03871.53	1.58	-0.08	-0.07	-0.20

The f' values are plotted and given as Figures 6.2 - 6.5, below. The theoretical data of Kissel [18] is also shown for comparison of the present results. It is seen from the figures that the present values of f' follow the trend as suggested by the theory.

Table 6.3: Photo effect cross-sections(σ_{tot}), imaginary part (f'') and real part (f') of the anomalous scattering factor for *Nb*

Energy	σ_{tot}	f''	Real Part, f'		
(keV)	($barns/atom$)		(KP)	(CM)	(CL)
15.74	03050.60	0.69	-1.25	-1.24	-1.38
16.58	02565.54	0.61	-1.57	-1.55	-1.70
17.44	02264.49	0.57	-1.95	-1.95	-1.94
17.63	02251.60	0.57	-2.05	-2.04	-2.19
18.70	01815.86	0.49	-3.36	-3.34	-3.49
19.60	11617.53	3.26	-2.70	-2.69	-2.83
20.16	11748.50	3.39	-1.92	-1.91	-2.05
21.12	09862.71	2.98	-1.15	-1.13	-1.28
22.71	08024.48	2.61	-0.64	-0.63	-0.78
23.11	07647.82	2.53	-0.56	-0.55	-0.70
23.81	07009.49	2.39	-0.45	-0.44	-0.59
25.19	06171.24	2.23	-0.26	-0.24	-0.39
26.17	05411.60	2.03	-0.16	-0.15	-0.29
28.56	04223.08	1.73	-0.18	-0.17	-0.32

Table 6.4: Photo effect cross-sections(σ_{tot}), imaginary part (f'') and real part (f') of the anomalous scattering factor for *Mo*

Energy	σ_{tot}	f''	Real Part, f'		
(keV)	($barns/atom$)		(KP)	(CM)	(CL)
15.74	03457.03	0.78	-1.23	-1.21	-1.37
16.58	02946.55	0.70	-1.47	-1.46	-1.61
17.44	02357.94	0.59	-1.79	-1.77	-1.93
17.63	02507.31	0.63	-1.86	-1.85	-2.00
18.70	02069.78	0.55	-2.36	-2.35	-2.50
19.60	01615.59	0.45	-3.47	-3.45	-3.61
20.16	12003.42	3.46	-4.37	-4.36	-4.52
21.12	11652.32	3.52	-2.42	-2.41	-2.57
22.71	11039.44	3.59	-1.06	-1.04	-1.20
23.11	09731.60	3.22	-0.80	-0.78	-0.94
23.81	08831.08	3.01	-0.64	-0.62	-0.78
25.19	07539.93	2.72	-0.35	-0.33	-0.49
26.17	06726.03	2.52	-0.21	-0.20	-0.35
28.56	05491.10	2.24	0.22	0.24	0.08

Table 6.5: Photo effect cross-sections(σ_{tot}), imaginary part (f'') and real part (f') of the anomalous scattering factor for Pd

Energy	σ_{tot}	f''	Real Part, f'		
(keV)	$(barns/atom)$		(KP)	(CM)	(CL)
15.74	5157.81	1.16	-0.62	-0.60	-0.80
16.58	4320.94	1.03	-0.79	-0.77	-0.97
17.44	3711.01	0.93	-0.96	-0.94	-1.14
17.63	3680.77	0.93	-1.00	-0.98	-1.17
18.70	3277.15	0.88	-1.13	-1.11	-1.30
19.60	2781.17	0.78	-1.21	-1.19	-1.38
20.16	1997.02	0.58	-1.38	-1.36	-1.56
21.12	2361.90	0.71	-1.65	-1.63	-1.83
22.71	1456.54	0.47	-2.28	-2.26	-2.45
23.11	1974.49	0.65	-2.52	-2.50	-2.70
23.81	1685.94	0.57	-3.14	-3.12	-3.31
25.19	9406.66	3.39	-2.48	-2.46	-2.65
26.17	8585.47	3.22	-1.60	-1.58	-1.77
28.56	6046.47	2.47	-1.10	-1.08	-1.27

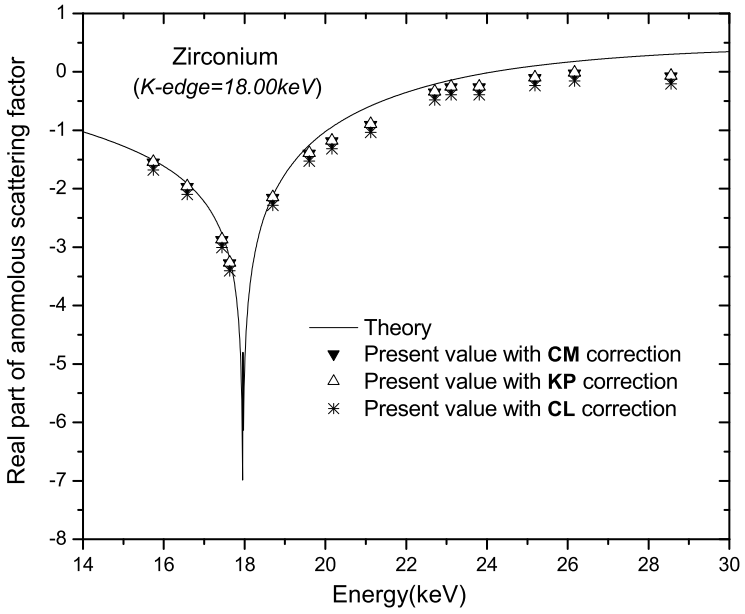

Figure 6.2: Plot of real part of the anomalous scattering factor as a function of photon energy around the K-edge of Zirconium.

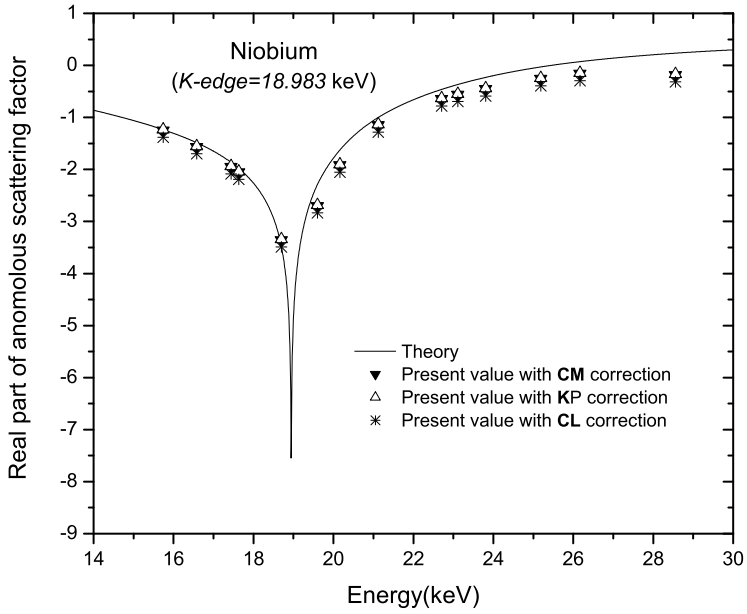

Figure 6.3: Plot of real part of the anomalous scattering factor as a function of photon energy around the K-edge of Niobium.

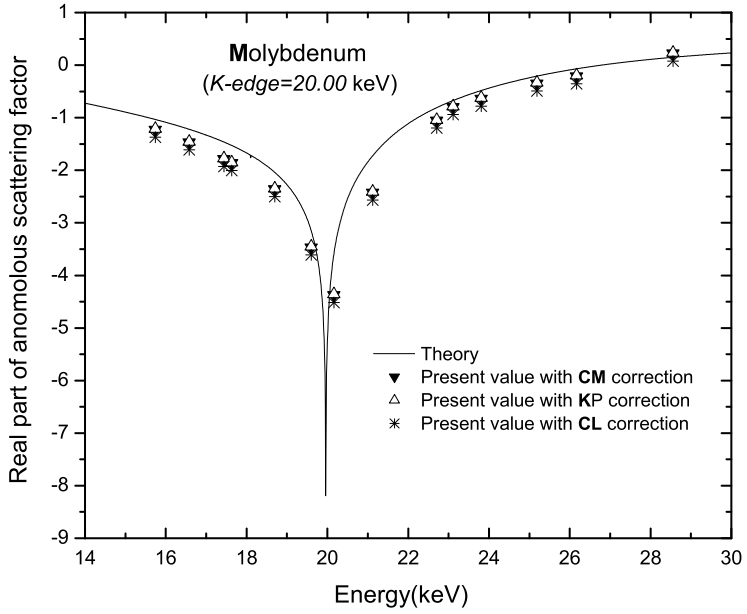

Figure 6.4: Plot of real part of the anomalous scattering factor as a function of photon energy around the K-edge of Molybdenum.

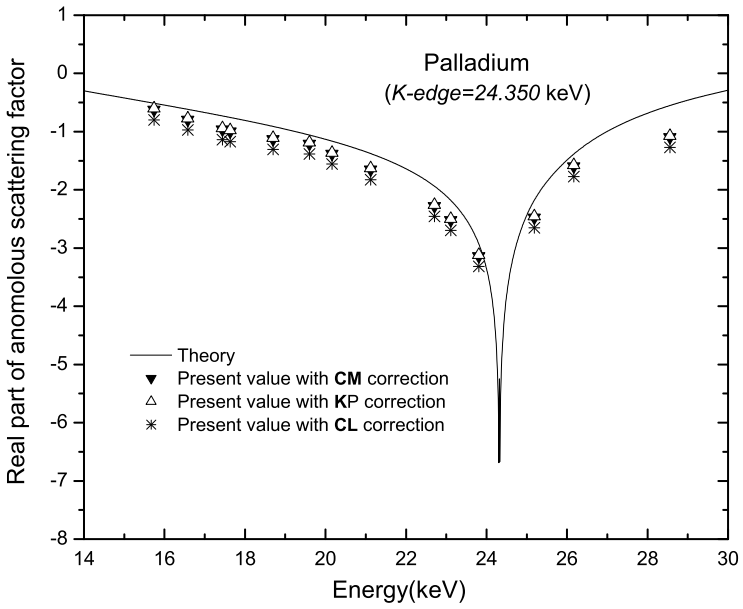

Figure 6.5: Plot of real part of the anomalous scattering factor as a function of photon energy around the K-edge of Palladium.

References

[1] D. T. Cromer and D. Liberman, *J. Chem. Phys* **53**,1898 (1970).

[2] R. W. James, *The optical principles of the diffraction of X-rays, Bell, London* (1962).

[3] B. E. Warren, *X-ray diffraction (Addison-Wesley : London)*(1945).

[4] M. Gavrila, *Inner shell processes (Ed. Bernd Craseman), New York.* 357 (1981).

[5] L. Kissel and R. H. Pratt *Atomic inner shell physics (Ed. Craseman. B) Plenum:New York.* (1983).

[6] D. C. Creagh and W. J. McAuley, Inter.Tables for Cryst. C (Ed. Wilson. A. J. C.), *(Kluwer Academic Publishers, Dordrecht)* 206 (1992).

[7] W. Thomas, *Naturwiss* **13**, 627 (1925).

[8] W. Kuhn, *f.Zeit Physik* **33**, 408 (1925).

[9] F. Reiche and W. Thomas, *Zeit. f. Physik* **34**,510 (1925).

[10] H. M. Nussenzveig, *Casuality and dispersion relations (Academic Press, New York*) 183 (1972).

[11] M. S. Wang, *Phys. Rev. A* **34**, 636 (1986).

[12] M. S. Wang and R. H. Pratt, *Phys. Rev. A* **28**, 3115 (1983).

[13] B. Zhou, L. Kissel and R. H. Pratt, *Nucl. instrum. Methods Phys. Res. B* **66**, 307 (1992).

[14] B. L. Henke. P. Lee, T. J. Tanaka, R. L. Shimambukuro and B. K. Fujikawa, *At. Data and Nucl. Data Tables* **27**, 1 (1982).

[15] L. Kissel and R. H. Pratt, *Acta Cryst.* A **46**, 170 (1990).

[16] J. H. Hubbell, Wm. J. Veigele, E. A. Briggs *et al*, *J.Phys. Chem. reference Data* **4**, 417 (1975).

[17] J. H. Hubbell and I. J. Overbo, *J.Phys. Chem. Reference Data* **8**, 69 (1979)

[18] Lynn Kissel, *Radiat. Phys. Chem.* **59**, 185 (2000)

Summary of results

Photon attenuation measurements are much in need, owing to its importance in many fields such as dosimetry, radiation biophysics, tomography, spectrometry and crystallography. In recent years, there has been renewed interest in the measurement of photon interaction measurements at low energies, especially energies close to absorption edges of elements.

In the present work, we have determined X-ray attenuation coefficients at different energies around K-edge of rare earth elements Sm, Eu, Gd, Tb, Dy and Er by using ^{241}Am (300 mCi) source. The energy variation around K-edge is accomplished through Compton scattering of photons on an aluminum target. The drawback of this technique, that the Compton scattered radiation will not be completely monochromatic is surmounted to a great extent by taking account of the energy spread and adopting an iterative procedure to extract the attenuation coefficients at the mean energy. The results are more defined to illustrate the abrupt variation of attenuation coefficients around K-edge than that of Polat *et al.*(2004) and consistent with the theoretical XCOM values within the quoted uncertainties. At the near K-edge energies investigated, our results do not indicate any breakdown of the mixture rule.

The determination of the attenuation coefficients near the K-absorption edges for the metals Zn, Nb, Mo and Pd at energies around their K-absorption edges is another set of measurements reported in this thesis. The method of Proton Induced X-ray Emission is used in this case. The energies chosen ranged from $15.74 to 28.56$ keV and were realized using secondary excitation from 25 micron thick foils of Zr, Nb, Mo, Rh, Pd, Cd and Sn. The results obtained agree

reasonably well with the theoretical XCOM values. This gives confidence in the measurement techniques adopted. The data of Tamura *et al.*(2002) for the range 17.22 - 20.56 keV are also seen to be consistent with our data. The present experiment, however covers a still wider range, 15.74 - 28.56 keV.

The attenuation measurements on Zr, Nb, Mo and Pd have also been done by using a radioactive source, ^{241}Am. As in the case of PIXE measurements, the energies chosen were in the range of $15.74 - 28.56$ keV and were obtained using secondary excitation from 25 micron thick foils of Zr, Nb, Mo, Rh, Pd, Cd and Sn. The experimental data obtained by this method also agree reasonably well with the XCOM values.

Keeping in view the fairly close comparison of the present results with theory, calculation of dispersion corrections to the forward Rayleigh scattering amplitude of the elements Zr, Nb, Mo and Pd had also been done. From the experimental values of attenuation coefficients the photoeffect cross sections (σ_{ph}) were derived by subtracting the sum of the corresponding coherent and incoherent scattering cross sections for the elements. These values of (σ_{ph}) yielded the imaginary part f'' of the anomalous scattering factor and taking account of the relativistic corrections, the f' values were obtained by evaluating the dispersion integral. The values are in fairly good agreement with the theoretical predictions.

Future Prospectives

The reasonably close comparison of theory with experimental data in the case of Compton scattering technique proves the reliability of the method of extraction of the attenuation coefficients for the rare earth compound absorbers at the discrete energies from the raw values, averaged over the spread in the energies. We feel therefore that the energy spread due to source, target and detector is to be taken into account, so that the variation of the attenuation coefficients around K-edge could be more defined.

The better accuracy of the PIXE results on attenuation measurements is worth mentioning. This is obviously due to the larger intensities of the incident

X-rays available with this technique as well as the relatively lower background levels. More investigations on X-ray attenuation near K-edge energies using the PIXE technique would be highly desirable for other elements also. A simple mechanical or an electronic set up to change the absorber from outside the PIXE chamber can save save our time and effort.

Scattering being an important mode of interaction of photons in the energy region of the present work, it is highly justified to study the anomalous scattering factor to the forward Rayleigh scattering amplitude. It is proposed to use the computer code developed for the purpose based on the attenuation measurements to determine the anomalous scattering factors for other elements also.

Appendix-I

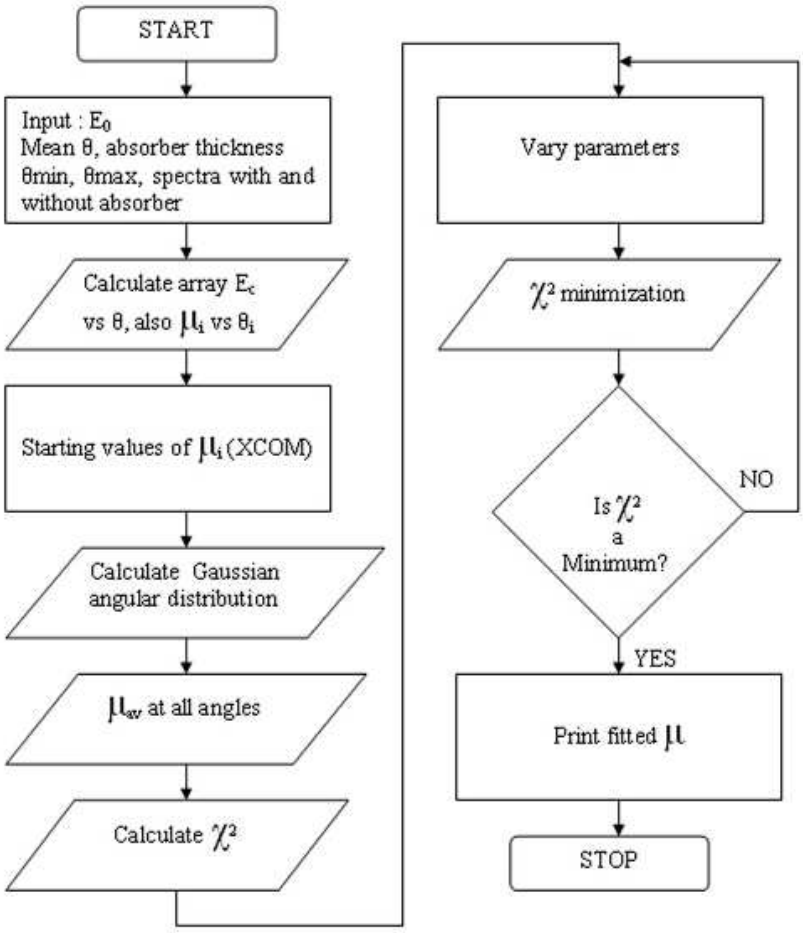

Figure 6.6: Flow chart of the computer program to extract the mass attenuation coefficient taking account of spreading in the dimensions of source, target and detector.

Appendix-II

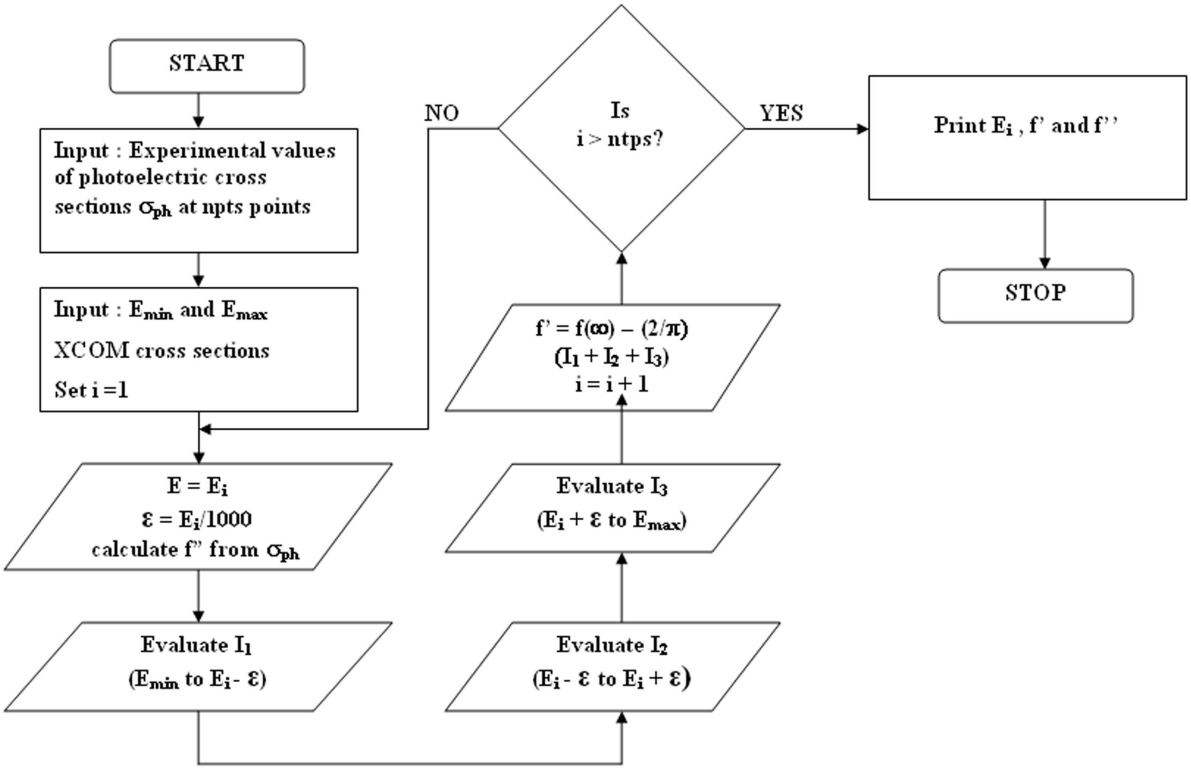

Figure 6.7: Flow chart of the computer program to find the real and imaginary parts of the anomalous scattering factor.